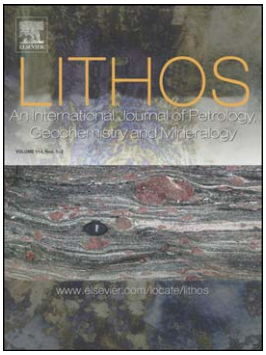

Syn-orogenic high-temperature crustal melting: Geochronological and Nd-Sr-Pb isotope constraints from basement-derived granites (Central Damara Orogen, Namibia)

J. Ostendorf, S. Jung, J. Berndt-Gerdes, F. Hauff

PII: S0024-4937(14)00011-5
DOI: doi: 10.1016/j.lithos.2014.01.007
Reference: LITHOS 3178

To appear in: *LITHOS*

Received date: 19 February 2013
Accepted date: 18 January 2014

Please cite this article as: Ostendorf, J., Jung, S., Berndt-Gerdes, J., Hauff, F., Syn-orogenic high-temperature crustal melting: Geochronological and Nd-Sr-Pb isotope constraints from basement-derived granites (Central Damara Orogen, Namibia), *LITHOS* (2014), doi: 10.1016/j.lithos.2014.01.007

Syn-orogenic high-temperature crustal melting: Geochronological and Nd-Sr-Pb isotope constraints from basement-derived granites (Central Damara Orogen, Namibia)

Ostendorf, J.[1, *#], Jung, S.[1], Berndt-Gerdes, J.[2], Hauff, F.[3]

[1] Fachbereich Geowissenschaften
Mineralogisch-Petrographisches Institut
Universität Hamburg
Grindelallee 48
20146 Hamburg, FRG

[2] Institut für Mineralogie
Universität Münster
Corrensstraße 24
48149 Münster, FRG

[3] IFM-GEOMAR
Research Division 4: Dynamics of the Ocean Floor
Wischhofstrasse 1-3
24148 Kiel, FRG

* present address:

Institut für Mineralogie
TU Bergakademie Freiberg
Brennhausgasse 14
09596 Freiberg, FRG

#: corresponding author: e-mail: joerg.ostendorf@mineral.tu-freiberg.de

Keywords

Granites; Damara orogen; Pre-Pan-African basement; U-Pb zircon geochronology; Nd-Sr-Pb isotopes

1. Introduction

The distribution of continental lithosphere has changed constantly through geological time, with larger continental masses periodically fragmenting into smaller crustal blocks and later re-amalgamating in different configurations as new supercontinents. The apparent random nature of this process hinders the reconstruction of ancient crustal terranes. Precambrian high-grade terranes may contain abundant granites that were derived from reworked older continental crust. Alternatively, granites in these terranes may represent differentiation products of juvenile material that originated directly from the mantle. Another possibility is the derivation of orogenic granitic magmas from an ancient source that contained both juvenile and older crustal components. Since granites often inherit geochemical and isotopic characteristics from their sources, their isotopic compositions can be used to reconstruct the geochemical composition and crustal history of granite-dominated terranes. Granitic melts form in different tectonic settings, from diverse sources and usually large amounts of crustal material are involved. These melts are often modified prior to emplacement or crystallization by a variety of processes that result in substantial geochemical variations among granitic plutons. However, depending on the actual degree of differentiation processes with or without crustal contamination after melt formation, the chemical and isotopic composition of the granites can still give valuable information about inaccessible portions of the deeper crust.

Large amounts of granites formed in the Central Zone of the Damara orogen of Namibia during Pan-African times (for a recent compilation see Miller, 2008). These include (i) syn-orogenic granites formed by partial melting of meta-igneous sources related to the Damara orogeny and pre-Damara basement (Jung et al., 2003; McDermott et al., 1996), (ii) syn-orogenic S-type granites formed by partial melting of upper crustal meta-sedimentary rocks (Jung et al., 2000; McDermott et al., 1996) and (iii) late-orogenic A-type granites (Jung et al., 2000). The exact geodynamic process that caused heat transfer and melting during collision of the

Kalahari craton and the Congo craton is still a matter of debate. Two contrasting models assume either a classical subduction zone environment (Barnes and Sawyer, 1980; Kasch, 1983; Miller, 1983) or an intracratonic failed rift environment (Kröner, 1982; Martin and Porada, 1977). During the last two decades, geochemical and isotope data for Damaran granites, together with precise U-Pb mineral ages have been presented. These data provide powerful constraints for the igneous evolution of the orogen. In this contribution, we present major element, trace element, isotope and geochronological data for granites and leucogranites from a basement-derived igneous complex in the Central Zone of the Damara orogen (Namibia); namely the Kubas igneous complex. The most recent compilation on Damaran granites (Miller, 2008) does not provide reliable age information and chemical and isotope data for the Kubas granites. Similarly, published work since the early 70´s have largely ignored this important small-scale igneous complex. The Kubas granites crop out in a transition zone between remobilized basement lithologies and metasedimentary rocks of the Nosib and Swakop Group (Damara Sequence). Therefore, it is important to work out potential sources that may have contributed to the chemical and isotope compostion of the granites. In addition, the data are used to place constraints on first-order processes. i.e. fractional crystallization with and without assimilation that may have modified their compositions.

2. Geological setting

The geology of the Damara orogen has been compiled in Miller (1983, 2008) and Gray et al. (2008). The Damara orogen exposes a deeply eroded cross section through a Pan African mobile belt. It consists of three branches that meet in a triple junction west of the Namibian coast. The NNW-SSE-trending Kaoko belt and the N-S-trending Gariep belt are situated along the Namibian coast whereas the ENE-WSW-trending Damara belt is located farther inland (Miller, 1983, 2008). The two coastal arms (Kaoko belt and Gariep belt) are considered to reflect the former Gondwana suture between South American and African cratons. The Damara belt s.s. is located between the Kalahari and the Congo cratons. It is still unclear whether the former basin between the two cratons rested on oceanic or continental crust. One model assumes an intracratonic failed rift with ensialic crust (Kröner, 1982; Martin and Porada, 1977) whereas another model assumes an oceanic basin with oceanic

lithosphere (Barnes and Sawyer, 1980; Kasch, 1983). The most important issue in this context is the size of the inferred ocean basin(s). The most recent compilation (Miller, 2008) suggests that the ocean basins are rather narrow features than wide areas underlayn by oceanic crust.

The major geological units of the Damara orogen are basement inliers with Archean and Proterozoic ages, shelf carbonates that surrounded the passive margins of the (ocean) basins between the cratons (Otavi Group), deepwater turbidites inside of the basins (Swakop Group) and foreland basin deposits in the Mulden and Nama Groups in the northern and southern parts of Namibia. The basal deposits that unconformably overlie the basement complexes are rift-related siliciclastic rocks of the Nosib Group (Gray et al., 2008; Miller, 1983, 2008). Quartz syenites, alkaline ignimbrites and alkali rhyolites in the upper Nosib Group constrain the minimum age to c. 750 Ma (Hanson, 2003; Hoffman et al., 1996; Jung et al., 2007). The overlying Otavi Group is dominated by carbonates that rimmed the basins between the cratons (Gray et al., 2008). The widespread Kuiseb Formation (upper Swakop Group) is composed of turbiditic greywackes and pelitic shists with calcsilicate bands (Miller, 1983, 2008). The ~300 km long Matchless amphibolites, which are intercalated with the pelitic to semipelitic succession of the upper Swakop Group, strikes parallel to the orogen and are interpreted to indicate probably minor ocean spreading (Schmidt and Wedepohl, 1983; Miller, 1983, 2008).

The ENE-WSW-trending Damara belt originated by convergence of the Congo and the Kalahari cratons. Based on stratigraphy, grade of metamorphism, structure and geochronology it can be divided into a Northern, Central and Southern Zone (Fig. 1). The Central Zone is dominated by granites, basement complexes and metasedimentary sequences (Miller, 1983, 2008) in which the basement is exposed in elongated domes that strike along the orogen. In general, the metamorphic grade of the Central Zone increase from east to west and reaches high grade conditions with local partial melting near the coast (Hartmann et al., 1983). The Central Zone is characterized by regional metamorphism of low to intermediate pressure. Peak metamorphic conditions were reached approximately 500 to 520 Ma ago just before or after the main deformation with temperatures of c. 700-750°C (Jung, 2000; Jung and Hellebrand, 2006; Jung and Mezger, 2003). There is, however, petrological and geochronological evidence that other metamorphic episodes occurred at c. 540 Ma and c. 490 to 470 Ma (Jung, 2000; Jung and Mezger, 2003). The Central Zone is

dominated by intrusive rocks ranging from gabbro/diorite: granodiorite/tonalite: granite/leucogranite in proportions of 2:2:96. The intrusive rocks range in age from c. 560 to c. 460 Ma (Miller, 2008) and crop out over an area of approximately 75,000 km^2. Based on their geochemical composition, most of the granites were derived from metasedimentary sources (Haack et al., 1982; McDermott et al., 1996; Jung et al., 2001) and metaluminous, amphibole-bearing granites, presumably generated by partial melting of meta-igneous sources (e.g. Jung et al., 1998), are rare. In addition, quartz diorites generated by partial melting of mafic lower crust occur also (Jung et al., 2002). Recent age determinations of structurally-controlled intrusive rocks (i.e. Longridge et al., 2011) indicated that in the south-western Central Zone, the main deformation (D2) occurred at 520-508 Ma and was coeval with high-grade metamorphism and granite intrusion (Jung and Mezger, 2003; Jung et al., 2003). This contrasts with age determinations elsewhere in the Central Zone that indicate early deformation around 550-540 Ma (Johnson et al., 2006) which is also coeval with metamorphism and antexis of basement rocks (Longridge et al., 2011). These age constraints are similar to a compilation of isolated ages provided by Gray et al. (2008). The Central Zone and the Southern Zone are separated by the Okahandja Lineament Zone. In the Southern Zone the Barrovian regional metamorphism increases from south to north and metamorphic conditions reached approximately 8 kbar with maximum temperatures of c. 600°C (Hartmann et al., 1983; Kasch, 1983).

3. Results

3.1 Field relationships and rock types

The Kubas igneous complex is located c. 25 km south of Usakos and has an extension of approximately 300 km² at the earth's surface (Fig. 2). It intruded into the metamorphic Abbabis complex as well as the Nosib and the Swakop Groups (Brandt, 1985; Schreiber, 1996). In general, the Kubas igneous complex consists of two different granite types, grey granites and red leucogranites, although the spatial distribution of these two types is not precisely known. According to Brandt (1985) the main mass of the granite complex is composed of grey granites that are locally intruded by reddish leucogranites; indicating that the red leucogranites are apparently younger than the grey granites. Based on differences of the trace element composition the red leucogranites are further subdivided into two subtypes (leucogranite I and leucogranite II). In addition to these granite types, numerous pegmatites of varying size transect the Kubas granites.

3.2 Mineralogy and petrography

The grey granites are composed of quartz, plagioclase, alkali feldspar (microcline/orthoclase) and biotite. Allanite, apatite and zircon occur as accessory phases. Minor muscovite occurs as an alteration product of K-feldspar. In general, the grey granites have a medium grain size except for some alkali feldspar phenocrysts with a grain size up to about 2 cm. Quartz and feldspar show undulatory extinction and often subgrain formation. Plagioclase is partly sericitized. Many of the plagioclase twinning lamellae change in width and taper at their ends. Some of the lamellae are bent. Alkalifeldspar is subordinately sericitized and Carlsbad twinning as well as microcline twinning can be found, sometimes within the same grain. For some of the grains, microcline twinning is observed solely in the centre of the crystal. Biotite often occurs in clusters, but single crystals are also present. Few biotite sheets are strongly bent. Muscovite occurs as alteration of plagioclase (sericitization) or in contact with biotite.

Both subtypes of the red leucogranites appear similar in their mineralogical compositions. They consist of quartz, plagioclase and alkali feldspar (microcline/orthoclase). Minor minerals are muscovite and biotite. Apatite, zircon and euhedral Mn-rich garnet are accessory minerals. Furthermore, partly digested

cordierite with sillimanite inclusions was observed (Fig. 3a). Undulatory extinction and subgrain formation in quartz is more apparent than in the grey granites and combinations of Carlsbad twinning and microcline twinning can be found in alkalifeldspar. Furthermore, weak sericitization is observed in K-feldspar but is not as obvious as in the grey granites. Well developed muscovite crystals are present in plagioclase and appear to be primary. Biotite generally occurs as cluster and parts of it are usually altered to chlorite (Fig. 3b). Some of the biotite sheets are bent. Garnet is subhedral and sometimes cracked.

4. Geochronology

4.1 Grey granites

Uranium-Pb zircon ages from the grey granites (samples 02/Ku07 and 02/Ku08) were obtained by LA-ICP-MS (Laser ablation - induction coupled plasma - mass spectrometry). Back-scattered-electron (BSE) and cathodoluminescence (CL) images of most of the investigated zircons showed predominantly igneous zonation patterns, however, many grains have an apparent core. Several different zircon age fractions could be observed (Table 2 and Fig. 4a): ~ 2.1 Ga to ~ 1.7 Ga (Fig. 4b), 1025 ± 17 Ma (Fig. 4c), 553.3 ± 8.4 Ma (Fig. 4d) and 502.4 ± 9.0 Ma (Fig 4e). The latter one consists of only three data points.

4.2 Red leucogranites

Separation of zircon that can be used for LA-ICP-MS dating was not possible due to the low amount of Zr in the samples. The Rb-Sr isotope ratios of the red leucogranites I plot on a well defined isochron (MSWD = 2.0) with an age of 512.9 ± 6.1 Ma (Fig. 5). Samarium-Nd isotope systematics yielded a similar but imprecise Sm-Nd whole-rock age of 497 ± 26 Ma (MSWD = 2.3) for the red leucogranites I. The leucogranites II have also elevated $^{147}Sm/^{144}Nd$ and $^{87}Rb/^{86}Sr$ ratios but these are not correlated with the $^{143}Nd/^{144}Nd$ and $^{87}Sr/^{86}Sr$ ratios, respectively. However, the samples plot at the lower end of the range defined by the red leucogranites I, suggesting some relationship between the two types of leucogranite.

5. Geochemistry

5.1 Major and trace element composition

The major and trace element whole rock composition of the granites from the Kubas igneous complex are shown in Table 1 and Figs. 6a and b. The grey granites have SiO_2 concentrations between 69.6 and 73.0 wt% and are lightly peraluminous with alumina saturation indices between 1.02 and 1.14 (ASI = molar Al/(Ca+Na+K)). The K_2O contents are higher than the Na_2O contents (K_2O/Na_2O: 1.24 - 1.68) and variations of K_2O and Na_2O are small (K_2O: 4.2 - 5.1 wt%, Na_2O: 3.0 - 3.4 wt%). Abundances of CaO, MgO, TiO_2 are rather uniform among the samples (CaO: 1.7 - 2.1 wt%, MgO: 0.7 - 1.1 wt%, TiO_2: 0.34 - 0.42 wt%). Ba is enriched relative to Rb and Sr, whereas Rb is enriched relative to Sr (Sr/Ba: 0.21 - 0.29, Rb/Ba: 0.38 - 0.51, Rb/Sr: 1.46 - 2.19). The Zr/Hf ratios vary between 34.7 and 37.1 and there is a well defined positive correlation between Zr and Hf. The variations of Rare Earth Elements (REE) of the grey granites are small and hence, the chondrite-normalized REE patterns are broadly similar (Fig. 7). Both, LREE and HREE are enriched with La_N/Sm_N ranging from 4.0 to 5.1 and Gd_N/Lu_N ratios ranging from 1.7 to 3.5. All grey granites show negative Eu anomalies (Eu/Eu*: 0.45 to 0.61). It is noteworthy, that correlations of major elements with SiO_2 (Fig. 6a) are virtually absent and the variation of the major elements is relatively small.

The red leucogranites can be subdivided into two subtypes. Both subtypes have high SiO_2 concentrations between 73.7 and 76.8 wt% and low MgO concentrations between 0.03 and 0.2 wt%. Furthermore, both types of red leucogranite are depleted in CaO, $Fe_2O_{3\,(total)}$ and TiO_2 (CaO: 0.5 - 1.1 wt%; $Fe_2O_{3\,(total)}$: 0.5 to 1.0; TiO_2: 0.01 - 0.06 wt%) (Fig. 6a). The ASI (alumina saturation index) is mostly similar to the grey granites (1.04 to 1.09) with the exception of sample 09/Ku01 which has a higher value of 1.22. The K_2O contents are generally higher than the Na_2O contents (K_2O: 4.2 - 4.9 wt%, Na_2O: 3.4 - 4.2 wt%; K_2O/Na_2O: 1.0 - 1.45). The red leucogranites I are enriched in Rb (395 - 424 ppm), Nb (39 - 56 ppm), Y (65 - 119 ppm) and U (9 - 29 ppm) and depleted in Sr (6 - 15 ppm) and Ba (17 - 90 ppm). Relative to the grey granites, they are enriched in Pb and depletd in Zr. The corresponding Rb/Sr and Rb/Ba ratios of the red leucogranites are high and the Sr/Ba ratios are low (Rb/Sr: 26 - 68, Rb/Ba: 4.4 – 25 Sr/Ba: 0.14 - 0.82) (Fig. 6b). Most of the chondrite-normalized REE patterns of the red leucogranites I are enriched in HREE relative to LREE (La_N/Yb_N: 0.4 - 0.5) and a prominent negative Eu

anomaly is observed (Eu/Eu* = 0.02 - 0.07) (Fig. 7). The Zr/Hf ratios of the red leucogranites I are low; ranging from 13.7 - 16.0.

The Sr contents of the red leucogranites II are less depleted than in leucogranites I (Sr: 18 - 55 ppm) whereas the Rb concentrations are slightly lower than those observed in the red leucogranites I. Consequently, the Rb/Sr ratios are significantly lower than in the red leucogranites I, ranging from 4.2 to 16.9. The Y, Nb and U contents are considerably lower than for the red leucogranites I (Y: 10 - 30 ppm, Nb: 8 - 22 ppm, U: 4 - 8 ppm). The REE patterns of the red leucogranites II are mostly unfractionated (La_N/Yb_N: 0.8 - 2.9) but the MREE are slightly depleted (Fig). The negative Eu anomaly is less well pronounced (Eu/Eu^* = 0.4 - 0.6) than in the red leucogranites I. The Zr/Hf ratios are slightly higher than in red leucogranite I and range from 17.4 to 21.5.

5.2 Sr, Nd and Pb isotopes

Strontium, Nd and Pb isotope analyses are reported in Table 3. The initial Sr and Nd isotope ratios of the grey granites are calculated for an age of 550 Ma. This age is assumed to reflect the magmatic age as shown by the U-Pb zircon ages. The initial $^{87}Sr/^{86}Sr$ ratios range from 0.718 to 0.720 and the initial ε_{Nd} values are strongly negative (ε_{Nd}: -16.1 to -17.6). The Nd model ages range from ~2.2 to ~2.5 Ga. The Pb isotope ratios of the grey granites obtained on acid leached feldspars are shown in Figure 9. The range in Pb isotopes is small with a notable variation in $^{207}Pb/^{204}Pb$ at virtually constant $^{206}Pb/^{204}Pb$ ratios and the samples plot above the Stacey and Kramers (1975) Pb evolution curve. The $^{206}Pb/^{204}Pb$ ratios range from 17.00 to 17.05, the $^{207}Pb/^{204}Pb$ ratios from 15.56 to 15.61 and the $^{208}Pb/^{204}Pb$ ratios from 37.98 to 38.17.

The initial Sr and Nd isotope ratios of the red leucogranites I and II are calculated to an age of 513 Ma. The initial $^{87}Sr/^{86}Sr$ ratios of the red leucogranites I range from 0.723 to 0.744 and for the red leucogranites II from 0.712 to 0.721. Because of the high Rb/Sr ratios of the red leucogranites, the accuracy of the calculated initial values is strongly dependent on the precision of the age and the accuracy of the Rb/Sr ratio. Hence, the reported values and inter sample variations are only approximations to the real values. The initial ε_{Nd} values of the red leucogranites I and II are similar and strongly negative ranging from -16.1 to -16.9 and from -13.6 to -19.1, respectively. The Nd model ages range from ~2.1 to ~ 2.5

Ga. The variations of Pb isotope ratios obtained on acid leached feldspars for both leucogranites cover a wide range of values (Table 3; Figure 9). In contrast to the grey granites, the leucogranites have substantial variations in $^{207}Pb/^{204}Pb$ and $^{206}Pb/^{204}Pb$ ratios. The $^{206}Pb/^{204}Pb$ ratios range from 17.17 to 18.05, the $^{207}Pb/^{204}Pb$ ratios from 15.58 to 15.67 and the $^{208}Pb/^{204}Pb$ ratios from 37.94 to 38.25. Like the grey granites, the leucogranites plot also above the Pb evolution curve defined by Stacey and Kramers (1975).

6. Discussion

The grey granites and the red leucogranites (I and II) are not directly genetically related, indicated by their different geological ages. However, all granite types of the Kubas igneous complex likely formed from similar sources but at different times, from melts modified by different processes.

6.1 Geochronology

The U-Pb zircon ages obtained on the grey granites gives the first precise age constraint for this igneous complex in the basement-dominated Central Zone of the Damara orogen. Inherited zircon cores give ages of c. 1.0 Ga and a range of ages between 1.8 to 2.1 Ga. Jacob et al. (1978) obtained an age of c. 2.0 Ga for the underlying Abbabis metamorphic complex and Kröner et al. (1991) and Longridge et al. (2011) have shown that remobilized basement rocks constitute an important fraction of the Pre-Damara rocks in the area with apparent ages of c. 1.0 Ga. Therefore, the inherited Proterozoic ages likely reflect the age of the underlying basement. Similarly, Johnson et al. (2006) reported inherited zircon grains from a Salem-type granite with an apparent Pb/Pb age of c. 1.9 Ga.

Zircon fractions yielding ages that are characteristic for the Damara orogenic episode give two age populations; one defining an age of 553 ± 8 Ma and another defining an age of 502 ± 9 Ma. We interpret the older age to reflect the main intrusion age of the grey granites. This interpretation is consistent with the U-Pb zircon age of 549±11 Ma (Jonson et al., 2006) from a nearby Salem-type granite. The younger age may reflect new growth of zircon at the time the leucogranites invaded the igneous

complex at 513±6 Ma which is constrained by the Rb-Sr whole rock age obtained on the leucogranites I. Rubidium-Sr dating of granites from the Damara orogen (Haack et al., 1980, 1982) have yielded a number of precise ages. Subsequent Pb-Pb zircon dating of some of these granites (Jung et al., 1998) have shown that the Rb-Sr ages could be similar or younger than the Pb-Pb ages. On the other hand, recent work on granulite-facies Proterozoic leucogranites from the Kaoko belt (Jung et al., 2012) has shown that even in granites that have undergone high-grade metamorphism, Rb-Sr ages can be similar to U-Pb zircon ages. Therefore, the younger Rb-Sr age obtained on the leucogranites may has geological significance. Alternatively, the younger U-Pb age of 502±9 Ma obtained on the grey granites correspond to limited new growth of zircon close to the inferred peak of regional metamorphism. This peak of regional metamorphism occurred at c. 500-510 Ma which is reflected by Sm-Nd and Lu-Hf garnet ages of unmigmatized metapelites or migmatized meta-igneous rocks occurring elsewhere in the basement-dominated part of the high-grade Central Zone of the Damara orogen (Jung et al., 2009; Jung and Hellebrand, 2006; Jung and Mezger, 2003). Similarly, Longridge et al. (2011) reported U-Pb zircon ages of 511±18 and 508±9 Ma on anatectic leucosomes which originated close to the peak of high-grade metamorphism.

6.2 Fractional crystallisation and assimilation processes

The chemical and isotopic composition of the grey granites is relatively homogenous with limited correlation of major and trace element composition with SiO_2 suggest that the grey granites have undergone only limited fractional crystallization. Radiogenic isotope compositions are not correlated with major and trace element data indicating the absence of assimilation processes. Therefore, we will use these samples to constrain the nature of the sources (see below).

The red leucogranites (I and II) were formed at the time when high-grade metamorphic conditions occurred in the Central Zone of the Damara orogen. They are products of highly fractionated melts which is shown by their high Rb/Sr and low Zr/Hf ratios and strongly modified chondrite-normalized REE patterns. Linnen and Keppler (2002) showed that fractional crystallization of metaluminous to peraluminous granite magmas leads to a decrease of Zr/Hf ratio in the most fractionated melts. Furthermore, the normative composition (Table 4) of both

subtypes of red leucogranites plots close to the minimum composition in the experimental haplogranite system at ~ 2 kbar (Johannes and Holtz, 1996) (Fig 10). It is suggested, that the two subgroups likely represent different evolutionary stages of a single differentiation process in which the red leucogranites I are probably products of more advanced fractional crystallisation processes than the red leucogranites II. This is shown by the higher Rb/Sr and lower Zr/Hf ratios, the strong enrichment of Nb, Y and U and the prominent negative Eu anomaly of the red leucogranites I. The chondrite-normalized REE pattern of the red leucogranites I and II can be explained by combined crystal fractionation/accumulation processes including major rock forming and accessory minerals such as plagioclase, garnet, apatite and allanite. The depletion of LREE of both subtypes of red leucogranites may be due to allanite fractionation; the negative Eu anomalies are likely a result of plagioclase fractionation, which was more advanced for the red leucogranites I than for the red leucogranites II. The relatively strong enrichment of the HREE and Y of the red leucogranites I is likely due to garnet accumulation. The slight MREE depletion of the red leucogranites II may be due to apatite fractionation. Crustal contamination of the red leucogranites I and II is indicated by the occurrence of cordierite with sillimanite inclusions and biotite clusters which are both likely remnants of upper crustal pelites (Fig. 3). Furthermore, the $^{206}Pb/^{204}Pb$-ratios of acid leached feldspars of the red leucogranites trend towards the composition of common pelitic metasediments from the Damara orogen (Fig 9).

6.3 Source of the granites

Slightly peraluminous granites like the grey granites can either form from metasedimentary or meta-igneous sources (Chappell et al., 1998; Chappell and White, 1992). The geochemical characteristics (enrichment of Ba and Rb relative to Sr, high K_2O, low CaO) of the grey granites indicate a crustal source rock. High Na_2O (> 3.5 wt.%), high CaO (>1.0 wt%) are unlike the values characteristic for pelitic sources (Na_2O: < 3.5 wt. %, CaO: < 1.2 wt. %; Miller, 1985). Similarly, Sr (~150 ppm) and Ba (> 500 ppm) abundances are also not characteristic for a pelitic parent (Sr: 70-100 ppm, Ba: 220-260 ppm; Miller, 1985). Comparison of the chemical composition of the grey granites with experimentally-derived partial melts (Patiño Douce, 1999) may suggest a greywacke source. Meta-greywackes from the Central Damara orogen have Na_2O, K_2O and CaO concentrations that are different to those

observed in metapelites (Na_2O: c. 2.3 wt%, K_2O: 2-3 wt%, CaO: 1.1-1.4 wt%; Jung et al., 1999). Although the Na_2O and CaO concentrations roughly match the concentrations observed in the grey granites, the K_2O abundances are too low to yield K_2O-rich granitic melts. Similarly, the low Sr (60-70 ppm) and Ba (80-210 ppm) contents of common Damaran metagreywackes (Jung et al. 1999) makes it unlikely that partial melting of such rocks can yield granites with 500-600 ppm Ba and ~ 150 ppm Sr. The largest problem is, that in the Damara orogen no metagreywackes have been observed that have ε_{Nd} values around -16 to -18 and unradiogenic Pb isotope compositions with $^{206}Pb/^{204}Pb$ ratios < 17.1. Hence, a derivation of the grey granites by partial melting of Damaran greywackes is unlikely.

Another possibility to yield Ba- and Sr-rich granitic melts is partial melting of pre-existing orthogneisses of granodioritic composition. If correct, and if modification of the chemical composition by fractional crystallization processes is negligible, the chemical composition of the granites should match the composition of experimentally-derived liquids. In Fig. 11, the composition of experimentally-derived liquids derived by partial melting of biotite gneisses (Patiño Douce and Beard, 1995) is shown. A comparison of chemical compositions of the experimental runs and the grey granites shows a close match between natural and experimental compositions. Low molar Al_2O_3/(MgO+FeO) and molar CaO/(MgO+FeO) values of the grey granites indicate that moderately high temperatures of c. 900°C were attained (Fig. 12). This temperature agrees well with the temperature estimate for the grey granites based on Al/Ti systematics (c. 900±15°C; calculated using the linear regression equation for igneous rock melting of Jung and Pfänder, 2007) and apatite thermometry (c. 920°C; Harrison and Watson, 1984) but is higher than the highest calculated Zr saturation temperature (Watson and Harrison, 1983) of 810°C (Table 5). Low molar Al_2O_3/(MgO+FeO) values of the grey granites relative to experimental results indicate that melting likely took place at pressures less than 10 kbar (Fig. 12), indicating relatively shallow melting of basement material. The degree of melting can be estimated from comparison with experimental investigations (Patiño Douce and Beard, 1995) and was probably between 10-20%. A more precise estimate on the degree of melting is not possible, however, due to the fact that the grey granites plot at the low-SiO_2 end defined by the experimental runs indicate that the degree of melting must be rather low. Experimental and thermal considerations indicated that 20% partial melting is a minimum estimate (i.e. Clemens and Vielzeuf, 1987).

However, it should be noted that K_2O abundances in granites may be sensitive to the degree of melting and early work by Roberts and Clemens (1993) and Clemens et al. (2011) indicated that high-K_2O granites can only be derived by melting of medium- to high-K_2O sources. Although the degree of melting can only be estimated indirectly by comparison with experimental data, it seems likely that the inferred parental melts of the grey granites were derived by moderate degrees of partial melting of a high-K_2O source.

Palaeoproterozoic Nd model ages, unradiogenic initial Nd isotope compositions and radiogenic Sr isotope compositions of the grey granites point to an ancient crustal source. Similar initial isotope values for different plutonic basement-derived rocks from the Central Zone of the Damara orogen are known (McDermott et al., 1996; Jung et al., 2003) and demonstrate that large amounts of pre-Damara basement were reworked during the Damara orogeny. The Pb isotope composition of acid leached feldspars also support the idea that the precursor rock of the grey granites had an ancient history in an environment that was characterized by high U/Pb ratios. Feldspars have very low μ ($^{238}U/^{204}Pb$)- and ω ($^{232}Th/^{204}Pb$)- values and hence, their Pb isotope composition points to the initial Pb isotope composition at the time when the rock last equilibrated. For granites, this event is most likely the time of intrusion. All samples plot above the Pb evolution curve according to Stacey and Kramers (1975). The large variation in $^{207}Pb/^{204}Pb$ ratios at almost identical $^{206}Pb/^{204}Pb$ ratios points to an ancient increase in the U/Pb ratio of the precursor of the grey granites. The unradiogenic $^{206}Pb/^{204}Pb$ ratios show that somewhere in the past, the source of the granites had undergone a stage where the U/Pb ratio of the source was lowered. As shown before, the grey granites have also higher $^{208}Pb/^{204}Pb$ ratios than the Stacey and Kramers (1975) model source. Relatively radiogenic $^{208}Pb/^{204}Pb$ ratios are likely due to ancient Th/Pb fractionation in the source of the grey granites. These $^{207}Pb/^{204}Pb$-$^{208}Pb/^{204}Pb$ isotope characteristics, that reflect U/Pb and Th/Pb fractionation in the past, can be connected with major crust-modifying processes (high-grade metamorphism and melting) that affected the source of the granites.

The chemical composition of the red leucogranites does not directly mirror the composition of their source rocks as the rocks are strongly fractionated. Similar initial Nd isotope ratios and old Nd model ages of 2.0 - 2.4 Ga point to a source similar to the source of the grey granites. This assumption is confirmed by the Pb isotope ratios

of the least modified samples of the red leucogranites which plot close to the Pb-isotope composition of the grey granites. From $^{207}Pb/^{204}Pb$ and $^{208}Pb/^{204}Pb$ isotope plots it is evident that the isotope composition of the leucogranites show a large variation in $^{206}Pb/^{204}Pb$ ratios. In particular, the array shown by the leucogranites point to the field occupied by Damaran metapelites (Jung, 2005), hence it is very likely that the leucogranites assimilated minor amounts of metapelitic material en route to the surface or during final emplacement. This is also compatible with the negative correlation between $^{87}Sr/^{86}Sr$ and $^{206}Pb/^{204}Pb$ (Fig. 13) in which the array depicted by the leucogranites evolves from high $^{87}Sr/^{86}Sr$ and low $^{206}Pb/^{204}Pb$ towards low $^{87}Sr/^{86}Sr$ and high $^{206}Pb/^{204}Pb$. This correlation also shows that (i) the red leucogranite II has probably the same source as the grey granites and (ii) contamination involves less evolved metasedimentary rocks of the Kuiseb Formation (Jung, 2005) rather than evolved metasedimentary rocks of the Etusis or Khan Formations (McDermott and Hawkesworth, 1990) that contains a large amount of recycled basement rocks. The inferred assimilation scenario is also compatible with the presence of cordierite with sillimanite inclusions and associated biotite clusters in these granites.

Although the correlations between $^{207}Pb/^{204}Pb$ and $^{206}Pb/^{204}Pb$ and also between $^{87}Sr/^{86}Sr$ and $^{206}Pb/^{204}Pb$ indicate assimilation processes, it is pertinent to ask why we see overall weak evidence for assimilation, although the isotopic and elemental contrast between the end members should be significant. The basement beneath the Damara orogen and the overlying sedimentary sequences have fairly high Sr and Nd abundances whereas Sr and Nd isotope compositions vary from strongly to moderately evolved. The grey granites have the highest Nd and Sr abundances and show virtually no signs of assimilation. The leucogranites have very low Nd and Sr abundances and assimilation of metasedimentary rocks or melts thereof with elevated Nd and Sr abundances (Jung 2005) must have a profound effect on the isotope compositions of the red leucogranites; yet very little field and petrographic evidence is observed. It seems that assimilation was very minor (a few percent), hence having little impact on the isotope composition.

7. Summary and conclusion

Two different types of granites intruded into the basement-dominated Kubas area (Central Damara orogen, Namibia). The syn-orogenic grey granites intruded at ~550 Ma and are among the oldest granites formed in the Damara orogen. They are probably uncontaminated; their chemical composition is relatively homogenous and hence, their composition likely mirrors their source which is assumed to be ancient pre-Damara basement. Based on a fairly good correlation of chemical data from experimental investigations and the grey granites, the source is likely a common biotite-bearing gneiss of granodioritic composition. The unradiogenic Pb isotope composition obtained on feldspar separates as well as evolved initial Sr and Nd isotopic compositions and inherited ancient U-Pb zircon ages also points to a pre-Damara basement source.

The red leucogranites are subdivided into two subgroups because of different trace element compositions. They formed at ~510 Ma at the time when high-grade peak metamorphic conditions prevailed in the Central Zone of the Damara orogen. Both subgroups of the red leucogranites likely formed from a source similar to the source of the grey granites. The chemical composition of both leucogranite subgroups changed after melt formation due to fractional crystallization processes; the red leucogranites I are likely products of more advanced differentiation processes than the red leucogranites II. During movement through or stagnation within the crust, minor assimilation of mid crustal metapelites occurred.

An important point to consider is why are there two separate melting events, separated by c. 40-50 Ma and why are the melting products somewhat different. Geochronological data obtained on metamorphic rocks and early syn-orogenic granites indiate that a first peak of metamorphism occurred at c. 540 Ma (Jung and Mezger, 2003) or slightly earlier (Longridge et al., 2011). This first metamorphic peak is associated with crustal thickening and shortening (Johnson et al., 2006; Longridge et al. 2011) and the grey granites are likely an outcome of this orogenic event where suitable basement sources are depressed at greater depths and hence were subjected to higher temperatures. The main peak of metamorphism (or a second peak related to reheating) occurred probably at c. 500 Ma (Jung and Mezger, 2003; Jung and Hellebrand, 2006, Jung et al. 2009; Longridge et al., 2011). At this time, lower granulite facies conditions were reached at mid-crustal levels and the red leucogranites studied here are melting products of fusible basement lithologies which are now, due to orogenic folding and stacking of crustal sheets, part of the mid crust.

The leucogranites are highly fractionated rocks but their precursor granites must be similar in composition than the grey granites, at least from an isotope persepective. There is no reason to believe that the contrasting chemical composition of both granite types is related to different genetic processes during melting, instead the chemical composition of the red leucogranites has been achieved due to extensive fractional crystallisation of an unexposed primary granite magma. The observation that two apparently similar granites are generated at two different times can be explained with the presence of limited amounts of water in the early history that aided melting of felsic basement rocks producing the grey granites. Later, when much of the water was expelled, more melting was possible due to rising metamorphic temperatures but apparently only limited amounts of granite was produced at that time. Note, however, that during the melting events both types of granitic melts were likely not water-saturated as those melts are unable to move through the crust. It is concluded that the grey granites are related to crustal thickening and heating of mid-crustal levels whereas the precursor rocks of the red leucogranites are related to crustal shearing and probably limited extension (Longridge et al., 2011).

Two main factors may have controlled the generation of granitic melts in the central part of the Damara orogen, (i) considerable crustal thickening and (ii) the radiogenic character and high heat productivity of the protoliths involved in granite genesis. The composition of the crust in the Damara orogen is essentially felsic and, as a consequence, this crust was likely characterized by high radioactive heat production during orogeny. Haack et al. (1983) calculated average heat production ratios of 2.5-8.8 $\mu W\ m^{-3}$ for meta-igneous rocks from the Damara orogen. These values are much higher than those used in theoretical models of anatexis in tectonically thickened crust (England and Thompson, 1986; 0.9-1.3 $\mu W\ m^{-3}$). According to England and Thompson (1986), a 50% increase in internal heat production raises peak temperatures by 150-200^{o}C at the bottom of the crust and thickening of 1.5 to 2 times the crust must result in widespread anatexis at mid-crustal levels. It is also predicted that melting events lag behind initiation of thrusting several tens of millions of years (Patiño Douce et al., 1990; Zen, 1988). The amount of time depends on the number and thickness of depressed thrust sheets, the duration of the thickening event, the initial temperatures and the amount of water present. Although there are a number of uncertainties, such a view is compatible with the observation that the main period of crustal melting at c. 500 Ma (Jung and

Hellebrand, 2006; Jung et al., 2000; Jung and Mezger, 2003) in the Damara orogen occurred ~ 30-40 Ma after the first peak of metamorphism which occurred at c. 540 Ma or slightly earlier (Jung, 2000; Jung and Mezger, 2003; Longridge et al. 2011). It is therefore very likely that the Damaran Pan-African continental crust was enriched in heat-producing elements, making it a good candidate for the massive production of granite during an orogeny in which existing temperature gradients will be steepened by the high radioactivity of depressed upper crustal rocks.

Acknowledgements

The authors are grateful to E. Thun (Hamburg) for support in the laboratory. The geochronological and isotope work was done at the Institut für Mineralogie, Universität Münster and Klaus Mezger and Heidi Baier are warmly thanked for their hospitality, help and advice during the senior author´s stay in Münster. Marion Tichomirowa and co-workers at the Institut für Mineralogie, TU Bergakademie Freiberg, are thanked for support during acquisition of additional Rb-Sr isotope analyses. Careful reviews by Richard Hanson and an anonymous reviewer were helpful in revising the manuscript and are highly appreciated. Nelson Eby is thanked for editorial handling.

Appendix A. Analytical techniques

Granite samples of c. 3-5 kg were crushed to powder using a jaw crusher, rod mill and a vibration disk mill with an agate grinding set. Mineral fractions in the grain size of 100 - 300 µm were separated by sieving of the coarse granular material available after crushing with the rod mill. Magnetically susceptible minerals were removed with a Frantz® magnetic separator. Zircon was isolated through density separation with methylene iodide and c. 25 - 50 mg of high purity K-feldspar were separated from the less dense fraction by hand picking.

Uranium-Pb ages were measured by laser ablation ICP-MS at the Institut für Mineralogie, Westfälische Wilhelms-Universität, Münster with a ThermoFinnigan Element2 sector field ICP-MS coupled to a New Wave UP193HE ArF Excimer laser system. Details of operation conditions can be found in Kooijman et al. (2012). Before U-Pb analysis of the zircon grains, back scattered electron (BSE) and cathodoluminescenece (CL) images were taken with a JXA 8900 Superprobe electron microprobe.

Major elements and some trace elements were measured on fused lithium-tetraborate glass beads by standard XRF techniques using a Panalytical MagixPro at the Institut für Mineralogie, Universität Hamburg. Prior to analysis, loss on ignition (LOI) was determined gravimetrically after heating the samples at c. 1000°C for 3 hours in a muffle furnace. For some samples (02/Ku01-06, 09/Ku01, 09Ku09, 09Ku11, 02/Ku08, 02/Ku09, 02/Ku11, 02/Ku12, 09/Ku02, 09/Ku04 and 09/Ku05) trace elements including REE were measured at Actlabs, Canada via ICP-MS. Accuracy of the analyses was tested against several international rock standards. The precision of the XRF data is c. 1% for major elements and 5-10 % for trace elements at concentrations above 100 ppm and 10-20 % for concentrations less than 100 ppm (see Table 1). The precision of trace element measurements by ICP-MS is estimated to be 5-10% (Table 1).

For Rb-Sr and Nd whole rock isotope analysis the samples were digested in concentrated HF-HNO_3 in 3 ml Savillex® screw top PFA vials using standard techniques; samples analyzed via isotope dilution were spiked with a mixed $^{87}Rb/^{84}Sr$ tracer prior to digestion. Dissolved samples were dried and redissolved with 2.5 N HCl. Strontium and REE were separated with standard cation exchange columns using DOWEX® AG 50 W-X 12 or AG 50 W-X 8. Neodymium was separated by using HDEHP coated Teflon® columns using 0.12 N HCl. For Rb and Sr isotope

analysis via isotope dilution analysis the dried samples were redissolved in ~3 N HNO_3 and loaded onto Teflon® micro columns filled with EICHROM® Sr resin. Rubidium was rinsed from the columns with ~3 N HNO_3, dried and loaded with H_2O onto Re-double filaments; no further purification of Rb was undertaken before analysis. Strontium was rinsed with H_2O from the same micro columns. Strontium was loaded with a TaF_5 activator onto W single filaments. Nd was run with Re double filaments.

Strontium isotope whole rock analyses were carried out at the Institut für Mineralogie, Westfälische Wilhelms-Universität Münster with a Finnigan Triton multicollector thermal ionization mass spectrometer (MC-TIMS) (samples 02/Ku01, 02/Ku02, 02/Ku04, 02/Ku05, 02/Ku06, 02/Ku08, 02/Ku09, 02/Ku11, 02/Ku12) and at the Institut für Mineralogie, Freiberg with a Finnigan MAT262 MC-TIMS (samples 02/Ku03, 09/Ku01, 09/Ku02, 09/Ku04, 09/Ku05, 09/Ku09, 09/Ku11). The reproducibility of Sr-standard NBS987 was $^{87}Sr/^{86}Sr = 0.710213 \pm 0.000007$ (2σ, n=10) at Münster and $^{87}Sr/^{86}Sr = 0.710217$ +- 0.000051 (2σ, n = 4) at Freiberg. Furthermore, the $^{87}Rb/^{86}Sr$-ratios of leucogranite samples (02/Ku01 - 06, 09/Ku01, 09/Ku09, 09/Ku11) were determined via isotope dilution analysis at the Institut für Mineralogie, Freiberg using a mixed $^{87}Rb/^{84}Sr$ tracer. Sm-Nd whole rock isotope analyses were carried out at the Institut für Mineralogie, Westfälische Wilhelms-Universität Münster and at GEOMAR (Kiel), each with a Finnigan Triton MC-TIMS. Reproducibility of the La Jolla Nd-standard was $^{143}Nd/^{144}Nd = 0.511859$ +- 0.000007 (2σ, n = 10) at Münster and $^{143}Nd/^{144}Nd = 0.511850$ +- 0.000003 (2σ, n = 5) at Kiel. Strontium isotope ratios are normalized to $^{86}Sr/^{88}Sr = 0.1194$ and Nd isotope ratios are normalized to $^{146}Nd/^{144}Nd = 0.7219$.

Lead isotope analyses of high-purity feldspar separates were carried out at the Institut für Mineralogie, Westfälische Wilhelms-Universität Münster with a VG Sector 54 MC-TIMS (samples 02/Ku01, 02 Ku02, 02/Ku04, 02Ku05, 02/Ku06, 02/Ku08, 02/Ku09, 02/Ku11, 02/Ku12, M64, M68, M73) and at GEOMAR (Kiel) (samples 02/Ku03, 09/Ku01, 09/Ku04, 09/Ku09, 09Ku11). At both institutes, c. 25 mg separated feldspar were washed with a HCl-HNO_3 (3:1) solution on a hotplate for several hours to remove unsupported lead. After rinsing several times with ultrapure H_2O, feldspar was leached twice with a mixture of concentrated HF and HNO_3 and was subsequently, dissolved in concentrated HF and dried afterwards. After this treatment, the samples were redissolved in 6 N HCl and dried again. Separation of

Pb was carried out with Teflon® micro columns filled with DOWEX® AG 1 X 8 resin using established HBr/HCl techniques. Lead was load onto Re single filaments with silica gel and H_3PO_4. Lead analyses were corrected for mass fractionation with a factor of 0.11% per amu for analyses obtained in Münster and 0.12% per amu for analyses obtained at GEOMAR Kiel.

References

Barnes, S.-J., Sawyer, E.W., 1980. An alternative model for the Damara Mobile Belt: Ocean crust subduction and continental convergence. Precambrian Research 13, 297-336.

Boynton, W.V., 1984. Geochemistry of the rare earth elements: meteorite studies, in: Henderson, P. (Ed.), Rare Earth Element Geochemistry. Elsevier, Amsterdam, pp. 63-114.

Brandt, R., 1985. Preliminary report on the stratigraphy of the Damara Sequence and the geology and geochemistry of Damaran granites in an area between Walvis Bay and Karibib. Communications of the Geological Survey of South West Africa/Namibia, 1, 31-43.

Chappell, B.W., Bryant, C.J., Wyborn, D., White, A.J.R., Williams, I.S., 1998. High- and Low-Temperature I-type Granites. Resource Geology 48, 225-235.

Chappell, B.W., White, A.J.R., 1992. I- and S-type granites in the Lachlan Fold Belt. Transactions of the Royal Society of Edinburgh: Earth Sciences 83, 1-26.

Clemens, J.D., Stevens, G., Farina, F., 2011. The enigmatic sources of I-type granites: The peritectic connexion. Lithos 126, 174-181.

Clemens, J.D., Vielzeuf, D., 1987. Constraints on melting and magma production in the crust. Earth and Planetary Science Letters 86, 287-306.

England, P.C., Thompson, A., 1986. Some thermal and tectonic models for crustal melting in continental collision zones. Geological Society, London, Special Publications 19, 83-94.

Govindaraju, K., 1994. 1994 Compilation of working values and sample description for 383 geostandards. Geostandards Newsletter 18, 1-158.

Gray, D.R., Foster, D.A., Meert, J.G., Goscombe, B.D., Armstrong, R., Trouw, R.A.J., Passchier, C.W., 2008. A Damara orogen perspective on the assembly of southwestern Gondwana. Geological Society, London, Special Publications 294, 257-278.

Haack, U., Gohn, E., Hartmann, O., 1983. Radiogenic Heat Generation in Damaran rocks, in: Miller, R.McG. (Ed.), Evolution of the Damara orogen of South West Africa/Namibia.Geological Society of South Africa Special Publications, 11, 225-232.

Haack, U., Gohn, E., Klein, J.A., 1980. Rb/Sr ages of granitic rocks along the middle reaches of the Omaruru River and the timing of orogenetic events in the Damara Belt (Namibia). Contributions to Mineralogy and Petrology 74, 349-360.

Haack, U., Hoefs, J., Gohn, E., 1982. Constraints on the origin of Damaran granites by Rb/Sr and δ18O data. Contributions to Mineralogy and Petrology 79, 279-289.

Hanson, R.E., 2003. Proterozoic geochronology and tectonic evolution of southern Africa. Geological Society, London, Special Publications 206, 427-463.

Harrison, T.M., Watson, E.B., 1984. The behavior of apatite during crustal anatexis: Equilibrium and kinetic considerations. Geochimica et Cosmochimica Acta 48, 1467-1477.

Hartmann, O., Hoffer, E., Haack, U., 1983. Regional Metamorphism in the Damara Orogen: Interaction of Crustal Motion and Heat Transfer, in: Miller, R.McG. (Ed.), Evolution of the Damara orogen of South West Africa/Namibia. Geological Society of South Africa Special Publications, 11, 233-241.

Hoffman, P.F., Hawkins, D.P., Isachsen, C.E., Bowring, S.A., 1996. Precise U-Pb zircon ages for early Damaran magmatism in the Summas Mountains and Welwitschia Inlier, northern Damara Belt, Namibia. Communications - Geological Survey of Namibia 11, 47-52.

Jacob, R., Kröner, A., Burger, A., 1978. Areal extent and first U-Pb age of the Pre-Damaran Abbabis complex in the central Damara belt of South West Africa (Namibia). Geologische Rundschau 67, 706-718.

Jacobsen, S.B., Wasserburg, G.J., 1980. Sm-Nd isotopic evolution of chondrites. Earth and Planetary Science Letters 50, 139-155.

Janoušek, V., Farrow, C.M., Erban, V., 2006. Interpretation of Whole-rock Geochemical Data in Igneous Geochemistry: Introducing Geochemical Data Toolkit (GCDkit). Journal of Petrology 47, 1255-1259.

Johannes, W., Holtz, F., 1996. Petrogenesis and experimental petrology of granitic rocks. Springer.

Johnson, S.D., Poujol, M., Kisters, A.F.M., 2006. Constraining the timing and migration of collisional tectonics in the Damara Belt, Namibia: U-Pb zircon ages for the syntectonic Salem-type Stinkbank granite. South African Journal of Geology 109, 611-624.

Jung, C., Jung, S., Nebel, O., Hellebrand, E., Masberg, P., Hoffer, E., 2009. Fluid-present melting of meta-igneous rocks and the generation of leucogranites — Constraints from garnet major- and trace element data, Lu–Hf whole rock–garnet ages and whole rock Nd–Sr–Hf–O isotope data. Lithos 111, 220-235.

Jung, S., 2000. High-temperature, low/meduim-pressure clockwise P-T paths and melting in the development of regional migmatites: The role of crustal thickening and repeated plutonism. Geological Journal 35, 345-359.

Jung, S., 2005. Isotopic equilibrium/disequilibrium in granites, metasedimentary rocks and migmatites (Damara orogen, Namibia)—a consequence of polymetamorphism and melting. Lithos 84, 168-184.

Jung, S., Hellebrand, E., 2006. Trace element fractionation during high-grade metamorphism and crustal melting—constraints from ion microprobe data of metapelitic, migmatitic and igneous garnets and implications for Sm–Nd garnet chronology. Lithos 87, 193-213.

Jung, S., Hoernes, S., Masberg, P., Hoffer, E., 1999. The Petrogenesis of Some Migmatites and Granites (Central Damara Orogen, Namibia): Evidence for Disequilibrium Melting, Wall-Rock Contamination and Crystal Fractionation. Journal of Petrology 40, 1241-1269.

Jung, S., Hoernes, S., Mezger, K., 2000. Geochronology and petrogenesis of Pan-African, syn-tectonic, S-type and post-tectonic A-type granite (Namibia): products of melting of crustal sources, fractional crystallization and wall rock entrainment. Lithos 50, 259-287.

Jung, S., Hoernes, S., Mezger, K., 2002. Synorogenic melting of mafic lower crust: constraints from geochronology, petrology and Sr, Nd, Pb and O isotope geochemistry of quartz diorites (Damara orogen, Namibia). Contributions to Mineralogy and Petrology 143, 551-566.

Jung, S., Hoffer, E., Hoernes, S., 2007. Neo-Proterozoic rift-related syenites (Northern Damara Belt, Namibia): Geochemical and Nd–Sr–Pb–O isotope constraints for mantle sources and petrogenesis. Lithos 96, 415-435.

Jung, S., Mezger, K., 2003. Petrology of basement-dominated terranes: I. Regional metamorphic T–t path from U–Pb monazite and Sm–Nd garnet geochronology (Central Damara orogen, Namibia). Chemical Geology 198, 223-247.

Jung, S., Mezger, K., Hoernes, S., 1998. Petrology and geochemistry of syn- to post-collisional metaluminous A-type granites—a major and trace element and Nd–Sr–Pb–O-isotope study from the Proterozoic Damara Belt, Namibia. Lithos 45, 147-175.

Jung, S., Mezger, K., Hoernes, S., 2001. Trace element and isotopic (Sr, Nd, Pb, O) arguments for a mid-crustal origin of Pan-African garnet-bearing S-type granites from the Damara orogen (Namibia). Precambrian Research 110, 325-355.

Jung, S., Mezger, K., Hoernes, S., 2003. Petrology of basement-dominated terranes: II. Contrasting isotopic (Sr, Nd, Pb and O) signatures of basement-derived granites and constraints on the source region of granite (Damara orogen, Namibia). Chemical Geology 199, 1-28.

Jung, S., Mezger, K., Nebel, O., Kooijman, E., Berndt, J., Hauff, F., Münker, C., 2012. Origin of Meso-Proterozoic post-collisional leucogranite suites (Kaokoveld, Namibia): constraints from geochronology and Nd, Sr, Hf, and Pb isotopes. Contributions to Mineralogy and Petrology 163, 1-17.

Jung, S., Pfänder, J.A., 2007. Source composition and melting temperatures of orogenic granitoids: constraints from CaO/Na2O, Al2O3/TiO2 and accessory mineral saturation thermometry. European Journal of Mineralogy 19, 859-870.

Kasch, K.W., 1983. Continental collision, suture progradation and thermal relaxation: a plate tectonic model for the Damara orogen in central Namibia, in: Miller, R.McG. (Ed.), Evolution of the Damara orogen of South West Africa/Namibia. Geological Society of South Africa Special Publications, 11, 423-429.

Kooijman, E., Berndt, J., Mezger, K., 2012. U-Pb dating of zircon by laser ablation ICP-MS: recent improvements and new insights. European Journal of Mineralogy 24, 5-21.

Kröner, A., 1982. Rb-Sr geochronology and tectonic evolution of the Pan-African Damara Belt of Namibia, southwestern Africa. American Journal of Science 282, 1471-1507.

Kröner, A., Retief, E.A., Compston, W., Jacob, R.E., Burger, A.J., 1991. Single-grain and conventional zircon dating of remobilized basement gneisses in the central Damara belt in Namibia. S South African Journal of Geology 94, 379-387.

Linnen, R.L., Keppler, H., 2002. Melt composition control of Zr/Hf fractionation in magmatic processes. Geochimica et Cosmochimica Acta 66, 3293-3301.

Longridge, L., Gibson, R.L., Kinnaird, J.A., Armstrong, R.A., 2011. Constraining the timing of deformation in the southwestern Central Zone of the Damara Belt, Namibia. Geological Society, London, Special Publications 357, 107-135.Martin, H., Porada, H., 1977. The intracratonic branch of the Damara Orogen in South West Africa I. Discussion of geodynamic models. Precambrian Research 5, 311-338.

McDermott, F., Harris, N.B.W., Hawkesworth, C.J., 1996. Geochemical constraints on crustal anatexis: a case study from the Pan-African Damara granitoids of Namibia. Contributions to Mineralogy and Petrology 123, 406-423.

McDermott, F., Hawkesworth, C.J., 1990. Intracrustal recycling and upper-crustal evolution: A case study from the Pan-African Damara mobile belt, central Namibia. Chemical Geology 83, 263-280.

Michard, A., Gurriet, P., Soudant, M., Albarede, F., 1985. Nd isotopes in French Phanerozoic shales: external vs. internal aspects of crustal evolution. Geochimica et Cosmochimica Acta 49, 601-610.

Milisenda, C.C., Liew, T.C., Hofmann, A.W., Köhler, H., 1994. Nd isotopic mapping of the Sri Lanka basement: update, and additional constraints from Sr isotopes. Precambrian Research 66, 95-110.

Miller, C.F., 1985. Are Strongly Peraluminous Magmas Derived from Pelitic Sedimentary Sources? Journal of Geology 93, 673-689.

Miller, R.McG., 1983. The Pan-African Damara Orogen of South West Africa/Namibia, in: Miller, R.McG. (Ed.), The Damara Orogen. Evolution of the Damara orogen of South West Africa/Namibia. Geological Society of South Africa Special Publications, 11, 431-515.

Miller, R.McG. (Ed.), 2008. The Geology of Namibia. Volume 2: Neoproterozoic to Lower Paleozoic. Ministry of Mines and Energy, Geological Survey, Windhoek, Namibia, p. p. 320.

Patiño Douce, A.E., 1999. What do experiments tell us about the relative contributions of crust and mantle to the origin of granitic magmas? Geological Society, London, Special Publications 168, 55-75.

Patiño Douce, A.E., Beard, J.S., 1995. Dehydration-melting of Biotite Gneiss and Quartz Amphibolite from 3 to 15 kbar. Journal of Petrology 36, 707-738.

Patiño Douce, A.E., Humphreys, E.D., Dana Johnston, A., 1990. Anatexis and metamorphism in tectonically thickened continental crust exemplified by the Sevier hinterland, western North America. Earth and Planetary Science Letters 97, 290-315.

Pressley, R.A., Brown, M., 1999. The Phillips pluton, Maine, USA: evidence of heterogeneous crustal sources and implications for granite ascent and emplacement mechanisms in convergent orogens. Lithos 46, 335-366.

Roberts, M.P., Clemens, J.D., 1993. Origin of high-potassium, calc-alkaline, I-type granitoids. Geology 21, 825-828.Schmidt, A., Wedepohl, K.H., 1983. Chemical Composition and Genetic Relations of the Matchless Amphibolite (Damara Orogenic Belt), in: Miller, R.McG. (Ed.), The Damara Orogen. Evolution of the Damara orogen of South West Africa/Namibia. Geological Society of South Africa Special Publications, 11, 139-145.

Schreiber, U.M., 1996. The Geology of the Walvis Bay Area. Geological Survey of Namibia, p. 50.

Seth, B., Jung, S., Hoernes, S., 2002. Isotope constraints on the origin of Pan-African granitoid rocks in the Kaoko belt, NW Namibia. South African Journal of Geology 105, 179-192.

Stacey, J.S., Kramers, J.D., 1975. Approximation of terrestrial lead isotope evolution by a two-stage model. Earth and Planetary Science Letters 26, 207-221.

Watson, E.B., Harrison, T.M., 1983. Zircon saturation revisited: temperature and composition effects in a variety of crustal magma types. Earth and Planetary Science Letters 64, 295-304.

Zen, E.-a., 1988. Thermal modelling of stepwise anatexis in a thrust-thickened sialic crust. Earth and Environmental Science Transactions of the Royal Society of Edinburgh 79, 223-235.

Syn-orogenic high-temperature crustal melting: Geochronological and Nd-Sr-Pb isotope constraints from basement-derived granites (Central Damara Orogen, Namibia)

Ostendorf, J.[1, *#], Jung, S.[1], Berndt-Gerdes, J.[2], Hauff, F.[3]

[1] Fachbereich Geowissenschaften
Mineralogisch-Petrographisches Institut
Universität Hamburg
Grindelallee 48
20146 Hamburg, FRG

[2] Institut für Mineralogie
Universität Münster
Corrensstraße 24
48149 Münster, FRG

[3] IFM-GEOMAR
Research Division 4: Dynamics of the Ocean Floor
Wischhofstrasse 1-3
24148 Kiel, FRG

* present address:

Institut für Mineralogie
TU Bergakademie Freiberg
Brennhausgasse 14
09596 Freiberg, FRG

#: corresponding author: e-mail: joerg.ostendorf@mineral.tu-freiberg.de

Abstract

Major and trace element and Nd, Sr and Pb isotope data from c. 550 Ma-old grey granites and c. 510 Ma-old red leucogranites of the high-grade central part of the Damara orogen (Namibia) indicate a dominantly deep crustal origin. Moderately peraluminous grey granites are isotopically evolved (initial ε_{Nd}: c. -17) and were likely derived from meta-igneous sources with late Archaean to Paleoroterozoic crustal residence ages. Based on a comparison with experimental results, the granites were derived by partial melting of a granodioritic biotite gneiss at c. 900-950^{o}C and less than 10 kbar. Slightly peraluminous red leucogranites are also isotopically evolved (initial ε_{Nd}: -15 to -18) but have undergone extensive crystal fractionation coupled with minor contamination of mid crustal meta-pelitic material. Major and trace element data do not support closed-system fractional crystallization processes for all samples, however, some chemical features underline the importance of crystal fractionation processes especially for the leucogranites. Isotope data do not support mixing of different crust-derived melts or assimilation of crustal rocks by a mafic magma on a large scale. For the grey granites, unradiogenic Pb isotope compositions with substantial variation in $^{207}Pb/^{204}Pb$ at almost constant $^{206}Pb/^{204}Pb$, strongly negative ε_{Nd} values and moderately radiogenic Sr isotope compositions argue for an undepleted nature of the source. High Rb/Sr ratios of the red leucogranites permit a comparison with the grey granites but similar initial ε_{Nd} values indicate that the source of these granites is not fundamentally different to the source of the grey granites. The most acceptable model for both granite types involves partial melting of meta-igneous basement rocks of Archaean to Proterozoic age. The consistency of the chemical data with a crustal anatectic origin and the observation that the grey granites intruded before the first peak of high-grade regional metamorphism suggests that they intruded simultaneously with crustal thickening. The red leucogranites are interpreted to be a result of crustal melting during the main peak of regional metamorphism. The heating events that promoted melting of fertile deep-crustal rocks might have been caused by the inferred high heat productivity of heat-producing radioactive elements (Th, U, K) together with crustal thickening during the main periods of orogeny.

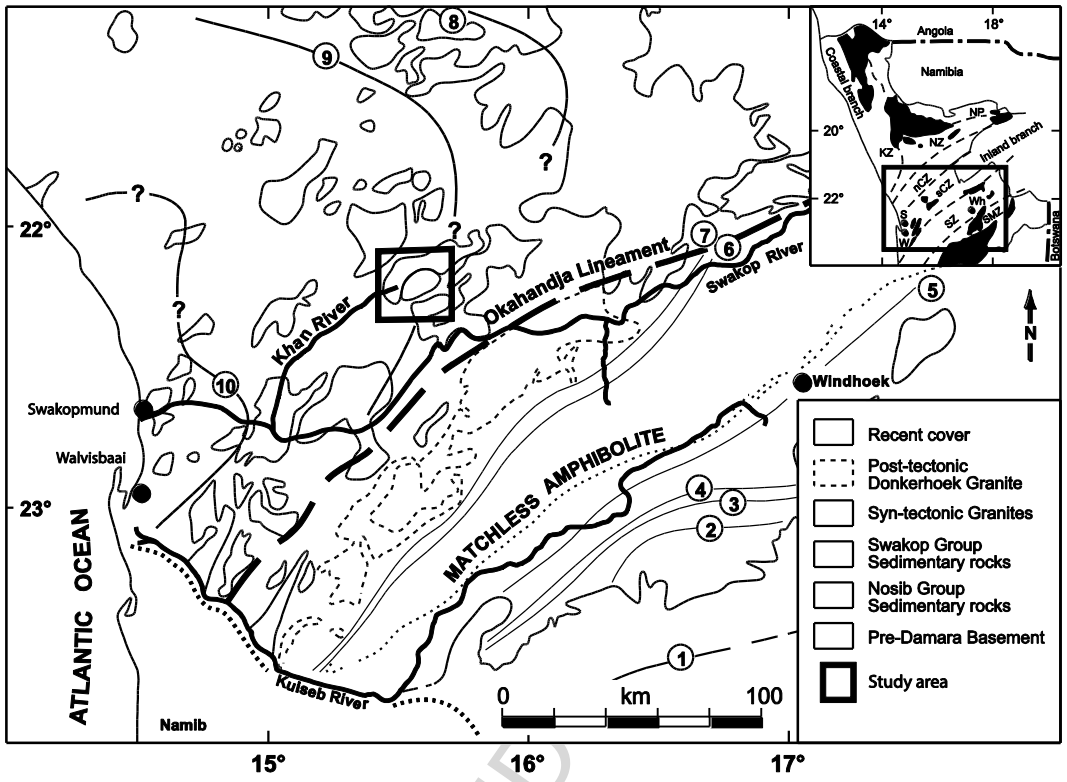

Figure 1

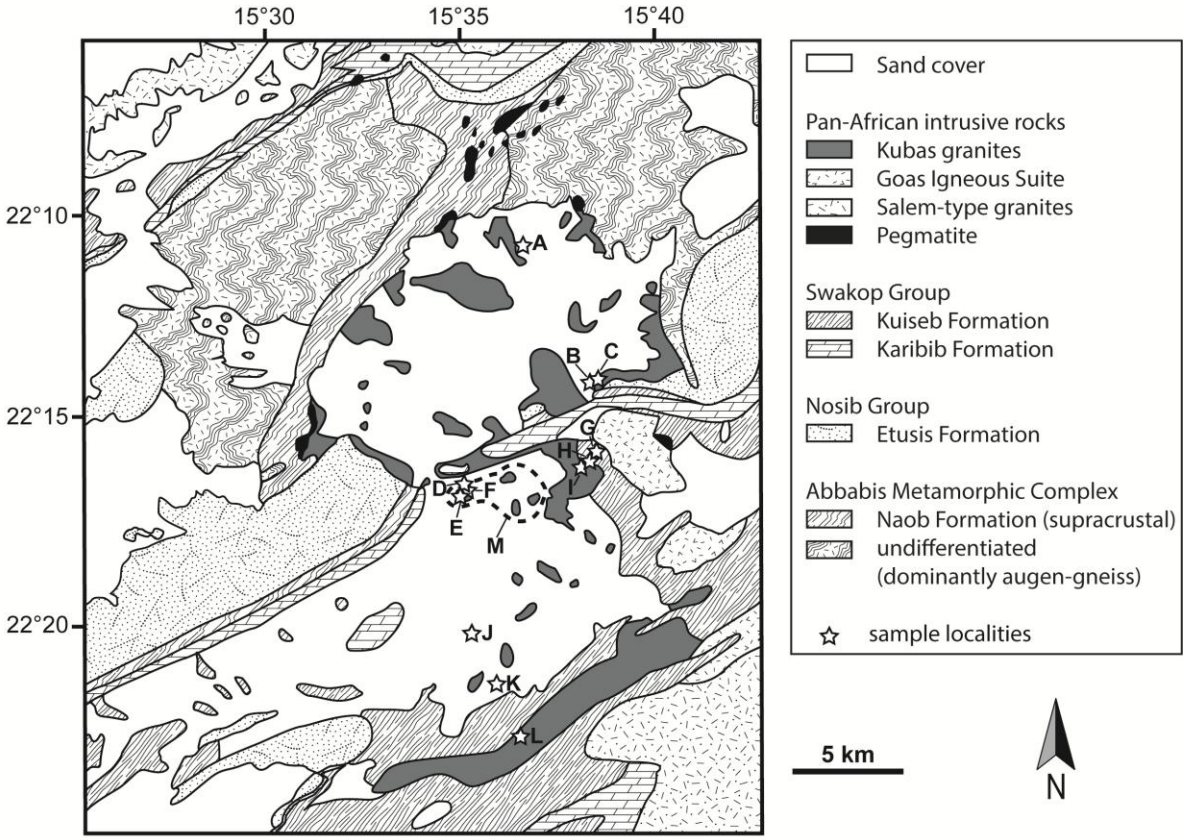

Figure 2

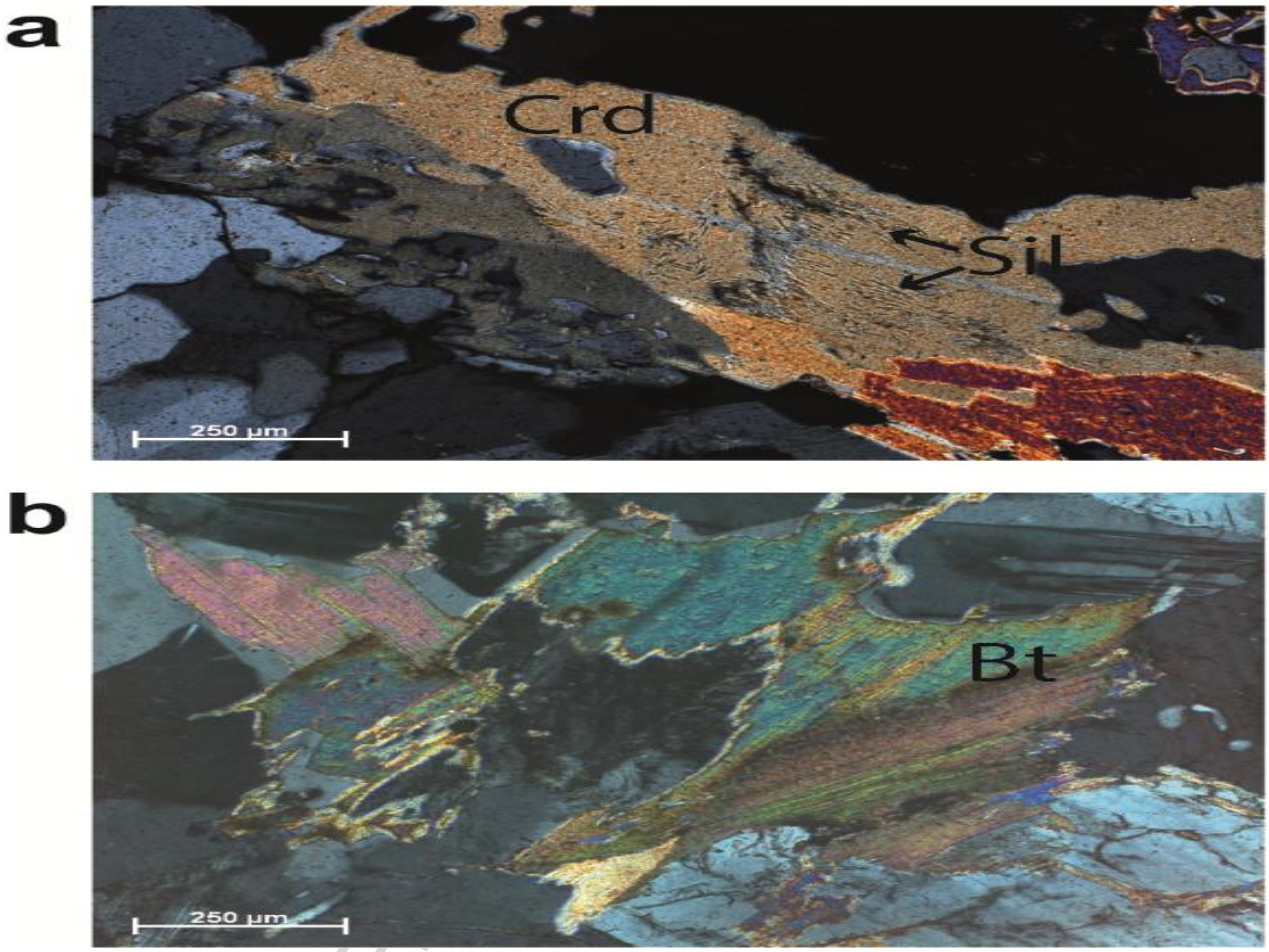

Figure 3

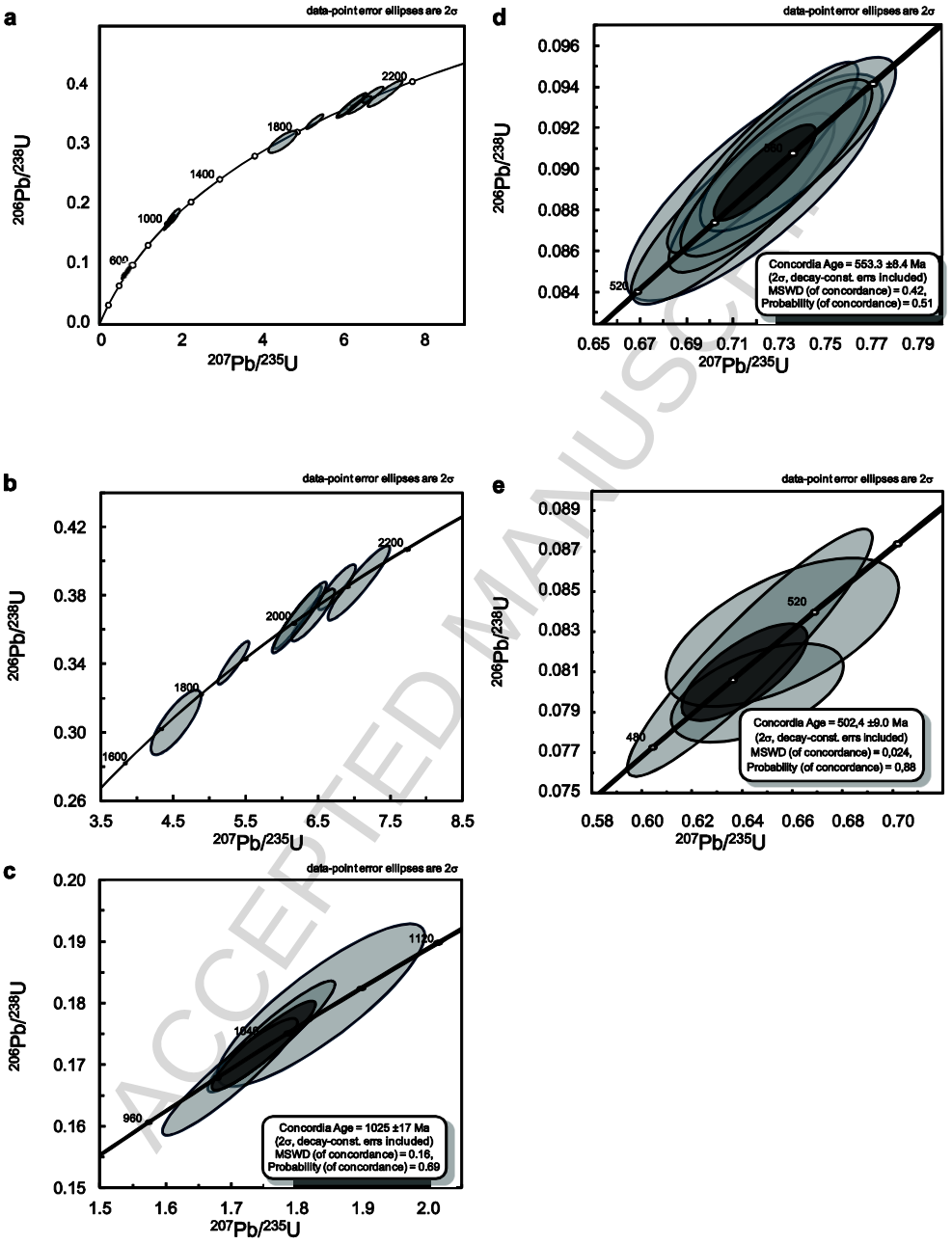

Figure 4

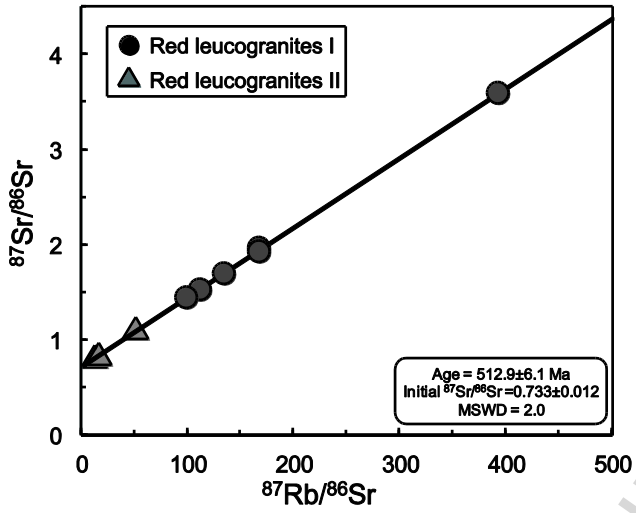

Figure 5

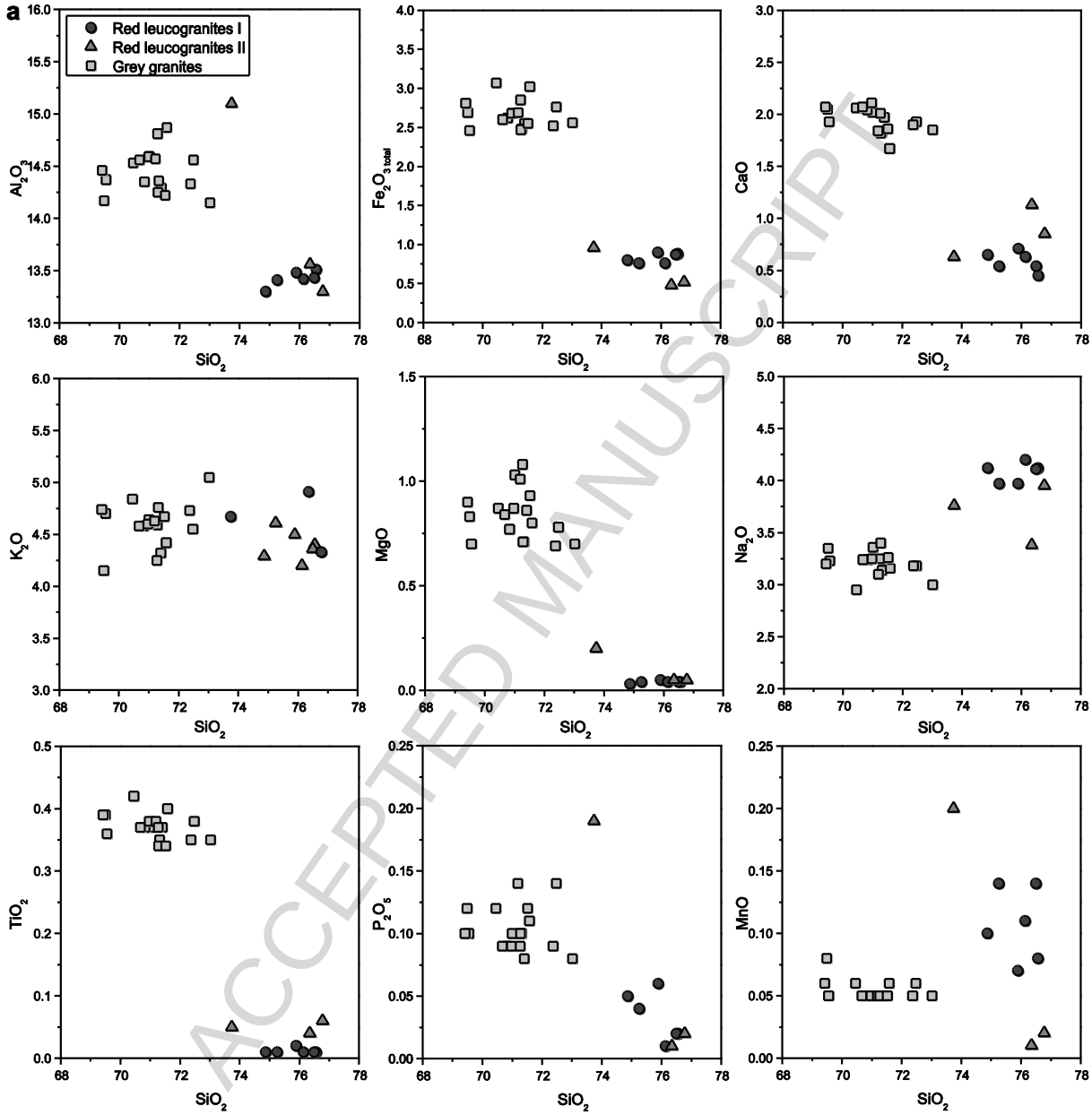

Figure 6a

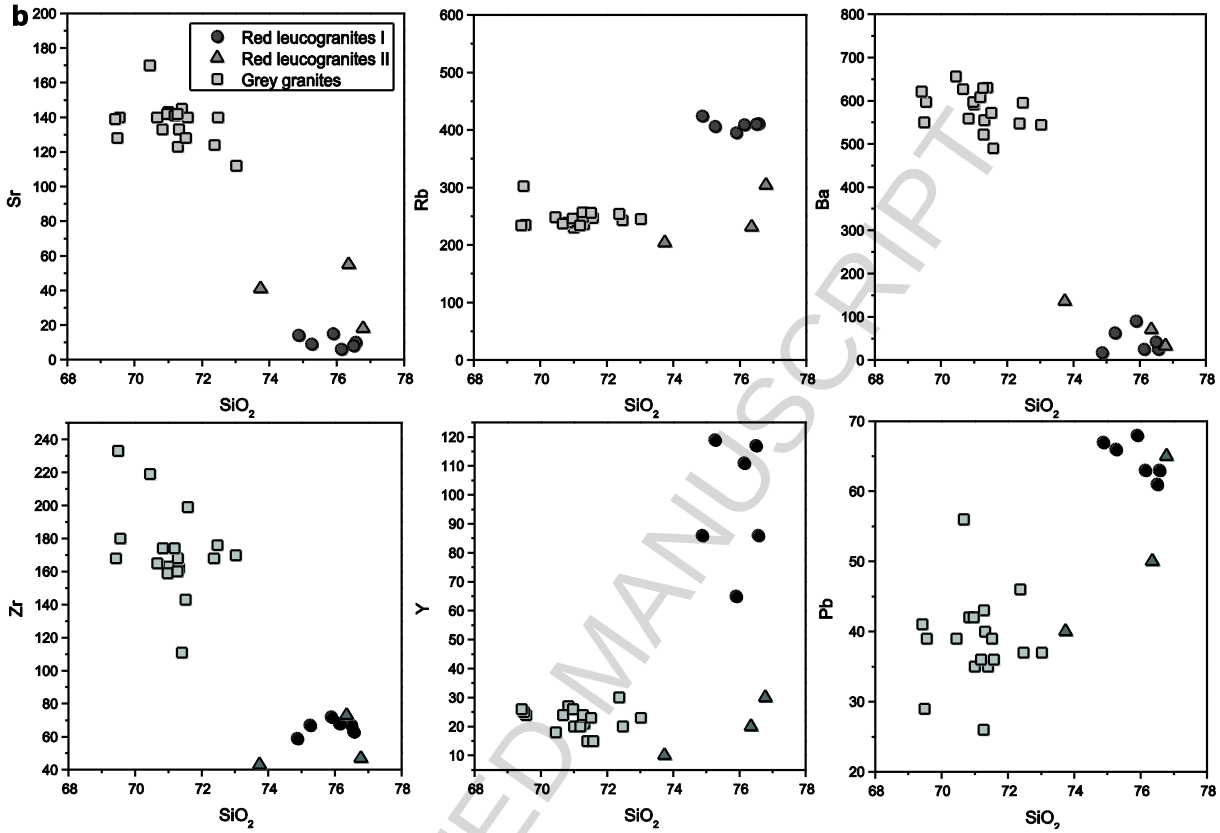

Figure 6b

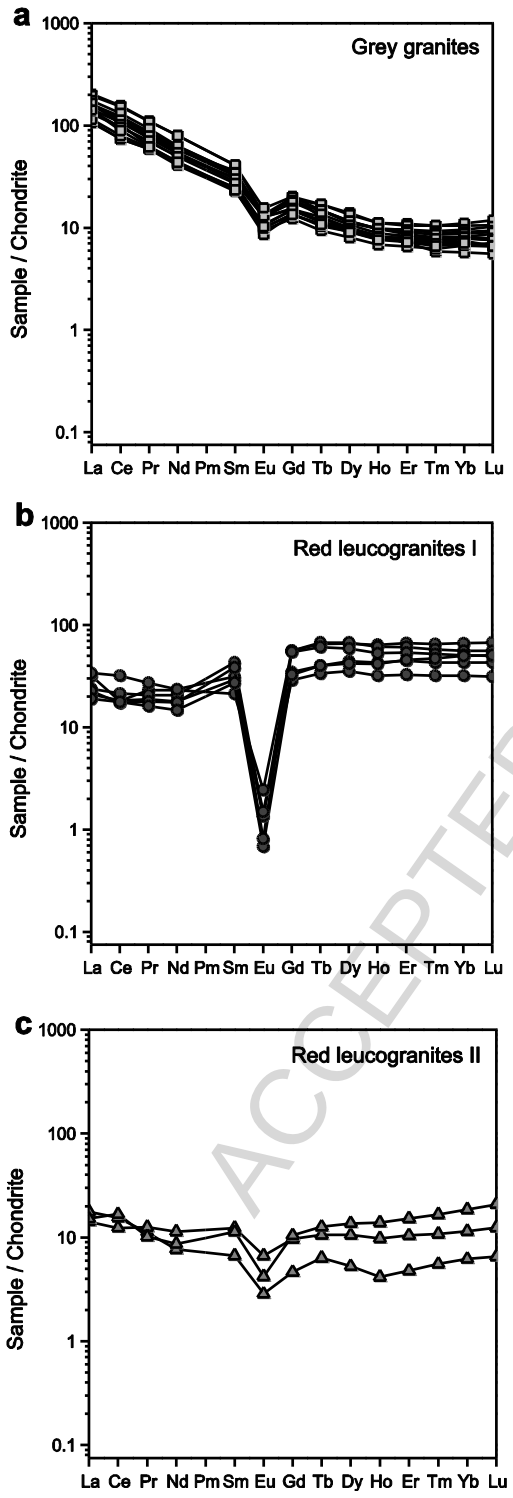

Figure 7

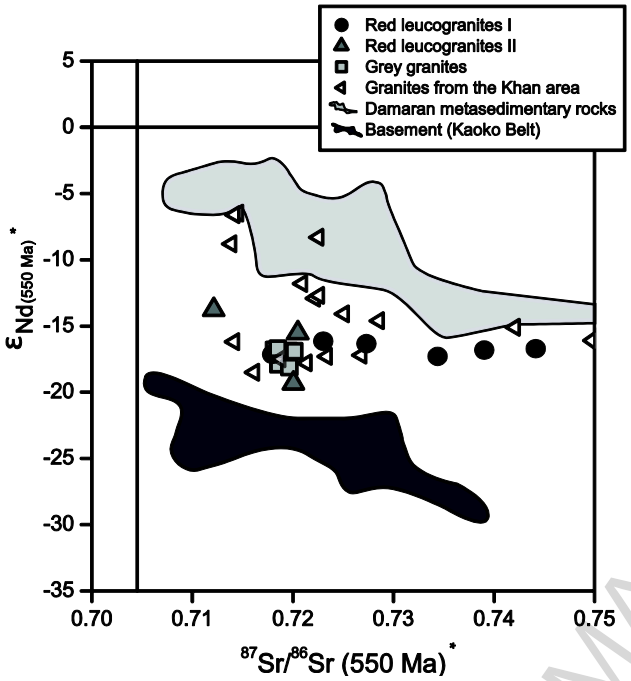

Figure 8

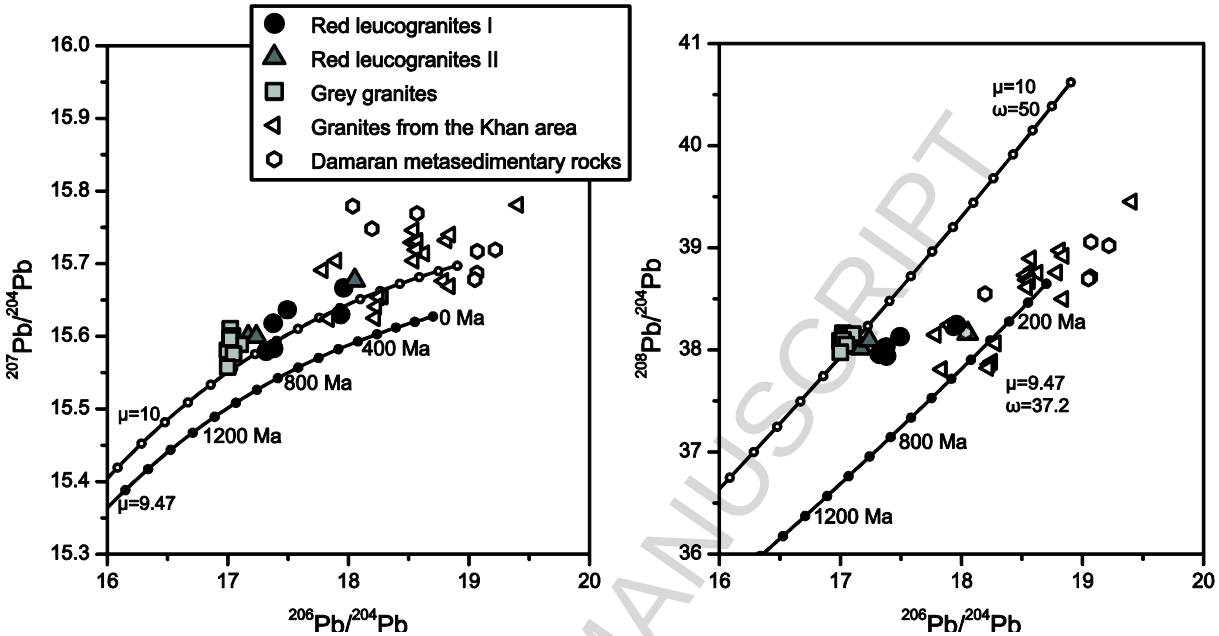

Figure 9

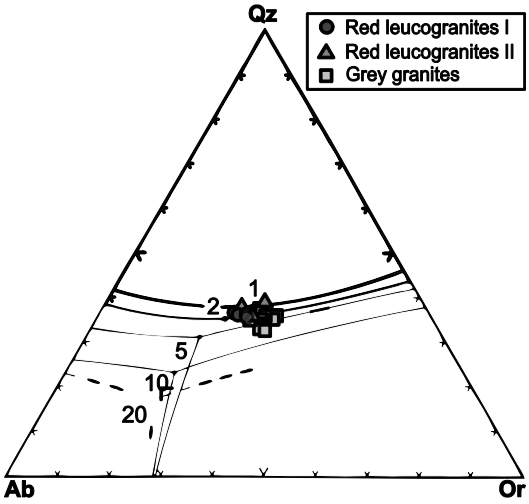

Figure 10

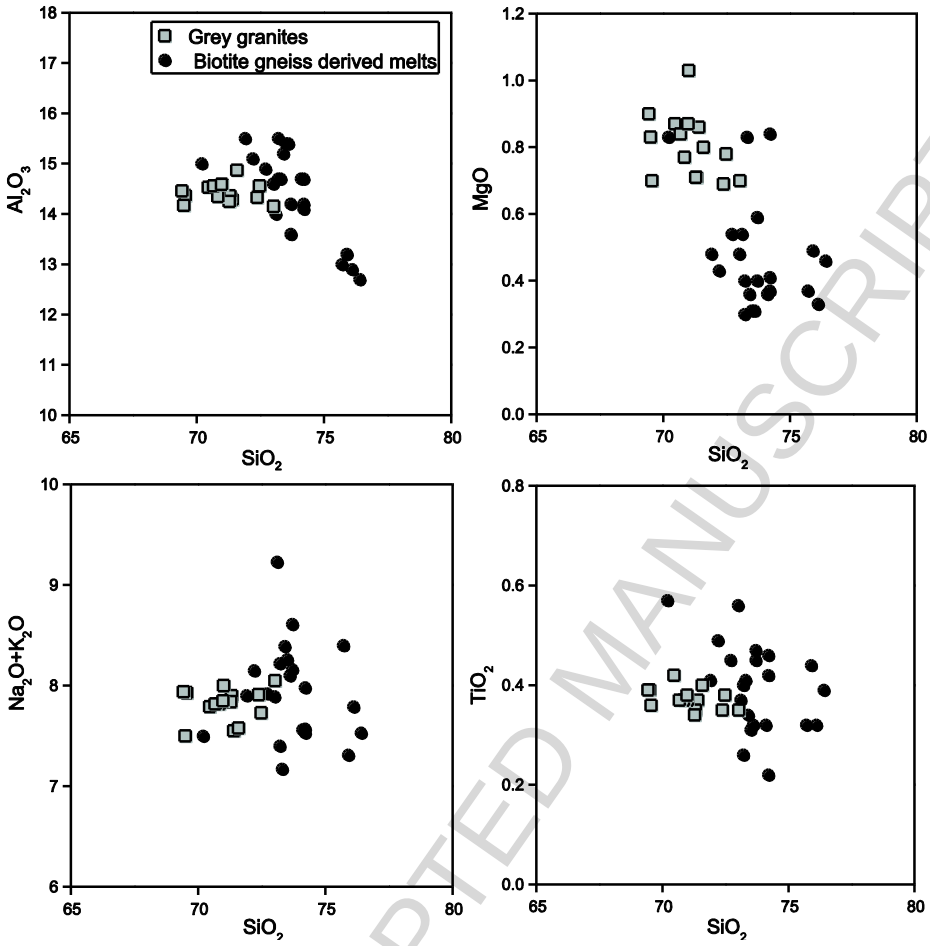

Figure 11

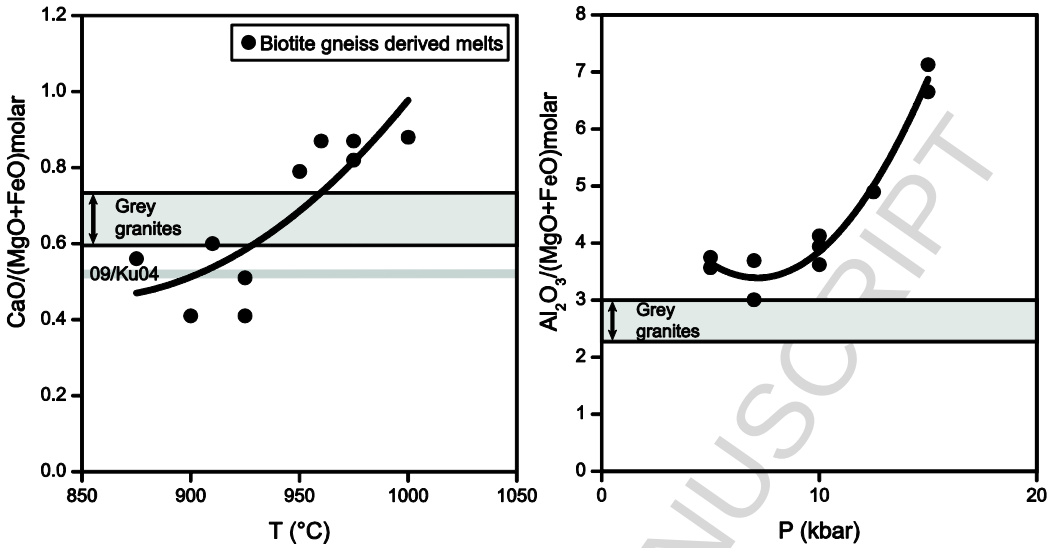

Figure 12

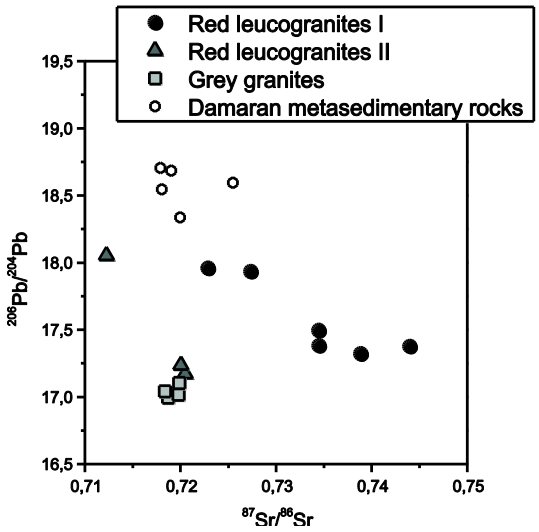

Figure 13

Fig. 1. Generalized geological map (modified after Jung and Mezger, 2003) showing the study area within the Central Zone of the Damara orogen, Namibia. Abbreviations in inset: KZ: Kaoko Zone, NP: Northern Platform, NZ: Northern Zone, nCZ: northern Central Zone, sCZ: southern Central Zone, SZ: Southern Zone, SMZ: Southern Margin Zone. Isograd map (Hartmann et al., 1983) gives the distribution of regional metamorphic isograds within the southern and central Damara orogen. Isograds: (1) biotite-in, (2) garnet-in, (3) staurolite-in, (4) kyanite-in, (5) cordierite-in, (6) andalusite ↔ sillimanite, (7) sillimanite-in according to staurolite-breakdown, (8) partial melting due to: muscovite + plagioclase + quartz + H2O ↔ melt + sillimanite, (9) K-feldspar + cordierite-in (10) partial melting due to: biotite + K-feldspar + plagioclase + quartz + cordierite ↔ melt + garnet. W: Walvisbay, S: Swakopmund, Wh: Windhoek.

Fig. 2. Simplified geological map of the study area (modified after Schreiber, 1996). Area denoted with dashed line indicates approximate area of M samples. Sample localities are explained in table 1.

Fig 3. Optical photomicrographs (crossed polarizers). (a) Cordierite with sillimanite inclusions in red leucogranite II, (b) biotite cluster in red leucogranite I. Crd: Cordierite, Sil: Sillimanite as fibrolite, Bt: Biotite.

Fig. 4. Concordia diagrams showing U-Pb zircon ages for the grey granites derived by LA-ICPMS. (a) All measured concordant ages between 2.1 Ga and 490 Ma, (b) concordant ages between 2.1 and 1.7 Ga, (c) concordant age of 1025 ± 17 Ma, (d) concordant age of 553.3 ± 8.4 Ma, (e) concordant age of 502.4 ± 9.0 Ma.

Fig. 5. Rb-Sr whole rock isochron for the red leucogranites I. Also shown is the Rb-Sr isotope composition of the red leucogranites II, plotting close to the isochron defined by the red leucogranites I.

Fig 6. (a) Major element plots and (b) selected trace element plots vs. SiO_2 for the grey granites and the red leucogranites I and II.

Fig 7. Chondrite-normalized REE plots for (a) grey granites, (b) red leucogranites I and (c) red leucogranites II. Normalization factors according to Boynton (1984).

Fig 8. $\varepsilon_{Nd(550\ Ma)}$ vs. $^{87}Sr/^{86}Sr$(550 Ma) diagram for grey granites and red leucogranites I and II of the Kubas igneous complex. Also shown is the composition of basement derived granites from the Khan area (Jung et al., 2003). Data for Damaran metasedimentary rocks are from Jung et al. (2003), Jung (2005) and McDermott and Hawkesworth (1990); data for basement rocks of the Kaoko belt are from Seth et al. (2002).

* initial Sr ratios and ε_{Nd}-values of the red leucogranites are calculated to an initial age of 513 Ma

Fig 9. Plot of $^{207}Pb/^{204}Pb$ and $^{208}Pb/^{204}Pb$ vs. $^{206}Pb/^{204}Pb$ isotope ratios of acid leached feldspar from the grey granites and the red leucogranites I and II of the Kubas igneous complex, Damaran metasedimentary rocks (Jung, 2005) and basement derived granites from the Khan area (Jung et al., 2003). One curve (dark spots) represents the average Pb growth curve according to Stacey and Kramers (1975), the other curve (bright spots) represents Pb evolution with higher μ ($^{238}U/^{204}Pb$) and higher ω ($^{232}Th/^{204}Pb$) values than shown by the Stacey and Kramers model. Tick marks represent 100 Ma intervals.

Fig 10. Normative Qz-Ab-Or compositions of the grey granites and red leucogranites I and II. Phase relations for the water saturated haplo granite system at 1, 2, 5, 10 and 20 kbar are according to Johannes and Holtz (1996).

Fig 11. Plots of Al_2O_3, MgO, Na_2O+K_2O, TiO_2 vs. SiO_2 for the grey granites of the Kubas igneous complex and for experimental melts derived by partial melting of biotite gneisses according to Patiño Douce and Beard (1995).

Fig 12. Plots of Al_2O_3/(MgO+FeO)molar vs. pressure and CaO/(MgO+FeO)molar vs. temperature for experimentally-derived liquids derived by partial melting of biotite gneisses (Patiño Douce and Beard, 1995). Also shown is the variation of the chemical composition of the grey granites.

Fig 13. Plot of $^{206}Pb/^{204}Pb$ vs. $^{87}Sr/^{86}Sr$ (init.) for the red leucogranites I and II and the grey granites. Data for Damaran metasedimentary rocks are from Jung (2005).

Table 1. Whole rock major element (in wt %) and trace element (in ppm) composition and sample localities for the grey granites and the red leucogranites I and II of the Kubas pluton.

Rock type	Red leucogranites I						Red leucogranites II		
Sample	02/Ku01	02/Ku02	02/Ku03	02/Ku04	02/Ku05	02/Ku06	09/Ku01	09/Ku09	09/Ku11
GPS	22°16´47 15°35´06	22°16´47 15°35´06	22°16´47 15°35´06	22°17´19 15°35´20	22°17´19 15°35´20	22°17´19 15°35´20	22°22´31 15°36´24	22°15´55 15°38.25	22°14´08 15°38´30
Sample locality in Fig 2	F	F	F	E	E	E	L	G	C
SiO_2	75.25	76.56	76.49	75.89	76.13	74.87	73.74	76.35	76.78
TiO_2	0.01	0.01	0.01	0.02	0.01	0.01	0.05	0.04	0.06
Al_2O_3	13.41	13.51	13.43	13.48	13.42	13.30	15.10	13.56	13.30
$Fe_2O_{3\ (total)}$	0.76	0.88	0.87	0.90	0.76	0.80	0.96	0.48	0.52
MnO	0.14	0.08	0.14	0.07	0.11	0.10	0.20	0.01	0.02
MgO	0.04	0.04	0.04	0.05	0.04	0.03	0.20	0.05	0.05
CaO	0.54	0.45	0.54	0.71	0.63	0.65	0.63	1.13	0.85
Na_2O	3.97	4.12	4.11	3.97	4.20	4.12	3.76	3.38	3.95
K_2O	4.61	4.40	4.36	4.50	4.20	4.29	4.67	4.91	4.33
P_2O_5	0.04	0.02	0.02	0.06	0.01	0.05	0.19	0.01	0.02
LOI	0.59	0.63	0.63	0.39	0.46	0.30	0.82	0.43	0.49
total	99.36	100.70	100.64	100.04	99.97	98.52	100.32	100.35	100.37
ASI	1.07	1.09	1.08	1.06	1.06	1.06	1.22	1.05	1.04
K_2O/Na_2O	1.16	1.07	1.06	1.13	1.00	1.04	1.24	1.45	1.10
Sc	10	10	7	14	12	9	8	7	7
V	<5	<5	<5	<5	<5	<5	<5	<5	<5
Ga	22	23	23	22	23	23	19	17	19
Rb	406	411	410	395	409	424	204	231	304
Sr	9	10	8	15	6	14	41	55	18
Y	119	86	117	65	111	86	10	20	30
Zr	67	63	67	72	68	59	43	73	47
Nb	47	56	50	39	46	45	8	10	22
Ba	63	25	42	90	25	17	136	71	33
Hf	4.8	4.6	4.7	4.5	4.7	4.3	2.0	4.1	2.7
Pb	66	63	61	68	63	67	40	50	65
Th	21.5	23.4	22.8	25.6	19.7	18.7	5.1	23.8	30.1
U	12.3	11.5	12.0	9.8	8.6	28.6	3.7	7.4	7.9
Rb/Sr	45.11	41.10	51.25	26.33	68.17	30.29	4.98	4.20	16.89
Rb/Ba	6.44	16.44	9.76	4.39	16.36	24.94	1.50	3.25	9.21
Sr/Ba	0.14	0.40	0.19	0.17	0.24	0.82	0.30	0.77	0.55
Zr/Hf	13.96	13.70	14.26	16.00	14.47	13.72	21.50	17.80	17.41
La	9.9	6.5	7.4	10.5	7.0	5.9	5.5	4.4	4.7
Ce	14.5	14.8	17.3	25.9	14.0	14.3	12.5	10.0	13.5
Pr	2.8	2.3	2.5	3.3	2.2	2.0	1.4	1.5	1.2
Nd	13.8	10.7	12.4	14.1	10.5	8.8	4.6	6.8	5.2
Sm	8.3	5.7	8.4	6.1	7.5	5.3	1.3	2.4	2.2
Eu	0.2	0.1	0.1	0.1	0.1	0.1	0.2	0.5	0.3
Gd	14.5	9.0	14.5	7.5	14.1	8.5	1.2	2.5	2.7
Tb	3.1	1.9	3.2	1.6	2.9	1.9	0.3	0.5	0.6
Dy	21.3	14.3	21.7	11.4	19.0	13.5	1.7	3.4	4.4
Ho	4.6	3.1	4.4	2.3	3.8	3.0	0.3	0.7	1.0
Er	14.0	9.4	12.8	6.9	11.3	9.6	1.0	2.2	3.2
Tm	2.1	1.4	1.9	1.0	1.7	1.5	0.2	0.4	0.5
Yb	13.9	9.0	11.7	6.7	10.6	10.4	1.3	2.4	3.9
Lu	2.17	1.39	1.80	1.01	1.61	1.63	0.21	0.40	0.67
Eu/Eu^*	0.07	0.04	0.03	0.05	0.02	0.02	0.51	0.61	0.39
La_N/Sm_N	1.50	0.72	0.55	1.08	0.59	0.70	2.66	1.15	1.34
La_N/Yb_N	0.48	0.49	0.43	1.06	0.45	0.38	2.85	1.24	0.81
Gd_N/Lu_N	0.83	0.80	1.00	0.92	1.09	0.65	0.71	0.78	0.50

Table 1 (continued)

Rock type	Grey granites								
Sample	02/Ku08	02/Ku09	02/Ku11	02/Ku12	09/Ku02	09/Ku04	09/Ku05	JR-1	recomm.
GPS	22°16´07 15°38´15	22°10´47 15°36´38	22°14´13 15°38´18	22°14´13 15°38´18	22°21´17 15°35´50	22°20´08 15°35´14	22°16´39 15°35´02		
Sample locality in Fig 2	H	A	B	B	K	J	D		
SiO_2	71.40	69.55	71.31	72.47	70.45	71.58	71.00		
TiO_2	0.37	0.36	0.35	0.38	0.42	0.40	0.37		
Al_2O_3	14.29	14.37	14.36	14.56	14.53	14.87	14.59		
$Fe_2O_{3\ (total)}$	2.55	2.46	2.48	2.76	3.07	3.02	2.68		
MnO	0.05	0.05	0.05	0.06	0.06	0.06	0.05		
MgO	0.86	0.70	0.71	0.78	0.87	0.80	1.03		
CaO	1.97	1.93	1.83	1.93	2.06	1.67	2.02		
Na_2O	3.23	3.23	3.14	3.18	2.95	3.16	3.36		
K_2O	4.32	4.70	4.76	4.55	4.84	4.42	4.64		
P_2O_5	0.08	0.10	0.10	0.14	0.12	0.11	0.10		
LOI	0.67	0.69	0.57	0.63	0.67	0.78	0.70		
total	99.79	98.14	99.66	101.44	100.04	100.87	100.54		
ASI	1.05	1.03	1.05	1.07	1.05	1.14	1.03		
K_2O/Na_2O	1.34	1.46	1.52	1.43	1.64	1.40	1.38		
Sc	5	9	11	5	11	9	15		
V	29	29	27	28	31	28	29	7	
Ga	20	20	20	21	20	22	20	17	17.6
Rb	248	235	236	243	248	247	230	254	257
Sr	145	140	133	140	170	140	143	30	30
Y	15	24	21	20	18	15	20	45.8	45,4
Zr	111	180	162	176	219	199	163	97	101
Nb	16	18	19	18	19	22	18	16	15.5
Ba	630	597	555	595	656	490	591	51	40
Hf	3.1	5.0	4.8	5.0	5.9	5.6	4.7	4.5	4.67
Pb	35	39	40	37	39	36	35	20	19.1
Th	23.4	21.5	28.4	29.7	35.6	32.0	24.9	26.8	26.5
U	3.4	4.0	7.6	5.2	3.1	4.6	6.2	9.3	9
Rb/Sr	1.71	1.68	1.77	1.74	1.46	1.76	1.61		
Rb/Ba	0.39	0.39	0.43	0.41	0.38	0.50	0.39		
Sr/Ba	0.23	0.23	0.24	0.24	0.26	0.29	0.24		
Zr/Hf		36.00	33.75	35.20	37.12	35.54	34.68		
La	44.6	40.2	44.1	49.1	62.6	60.6	47.7	20 .7	19 .7
Ce	86.5	77.6	87.2	94.3	126.0	123.0	93.1	48.3	47.1
Pr	9.2	8.4	9.5	10.1	13.5	13.3	10.0	5 .47	5.62
Nd	31.8	29.9	34.3	36.0	47.6	47.6	35.1	23.2	23.5
Sm	5.5	6.0	7.0	6.5	7.9	8.0	6.3	5.8	6.07
Eu	0.9	0.9	0.9	0.9	1.1	1.0	1.0	0.28	0.3
Gd	3.9	4.9	5.2	4.6	5.2	5.1	4.5	5.57	5.24
Tb	0.6	0.8	0.8	0.7	0.7	0.6	0.7	1.02	1.02
Dy	3.0	4.5	4.3	3.7	3.6	3.2	3.7	5.69	5.78
Ho	0.6	0.8	0.8	0.7	0.7	0.6	0.7	1.21	1.1
Er	1.5	2.3	2.2	2.0	1.8	1.5	2.0	4.03	3.78
Tm	0.2	0.3	0.3	0.3	0.3	0.2	0.3	0.7	0.67
Yb	1.4	2.2	2.3	2.0	1.7	1.2	1.9	4.8	4.49
Lu	0.23	0.34	0.38	0.33	0.28	0.18	0.30	0.70	0.71
Eu/Eu^*	0.61	0.53	0.45	0.53	0.54	0.47	0.55		
La_N/Sm_N	5.10	4.21	3.96	4.75	4.98	4.76	4.76		
La_N/Yb_N	21.48	12.32	12.93	16.55	24.83	34.05	16.93		
Gd_N/Lu_N	2.11	1.79	1.70	1.73	2.31	3.52	1.86		

Table 2. LA-ICP-MS U-Pb zircon analyses for the grey granites of the Kubas pluton (samples 02/Ku07 and 02/Ku08).

Analyis name	Ratios $^{206}Pb/^{238}U$	±2σ	$^{207}Pb/^{235}U$	±2σ	$^{207}Pb/^{206}Pb$	±2σ	Rho	Ages (Ma) $^{206}Pb/^{238}U$	±2σ	$^{207}Pb/^{235}U$	±2σ	$^{207}Pb/^{206}Pb$	±2σ
~2.1 - ~1.7 Ga													
Ku07-4-1	0.385	0.011	6.763	0.215	0.1275	0.0019	0.88	2099	50	2081	28	2064	26
Ku07-16-1	0.306	0.015	4.534	0.285	0.1076	0.0040	0.80	1720	76	1737	52	1759	68
Ku07-17-1	0.340	0.010	5.327	0.176	0.1135	0.0015	0.91	1889	50	1873	28	1856	24
Ku07-33-1	0.367	0.017	6.240	0.306	0.1233	0.0021	0.94	2015	80	2010	43	2005	30
Ku07-37-1	0.367	0.015	6.224	0.268	0.1230	0.0016	0.95	2015	71	2008	38	2000	23
Ku07-40-1	0.387	0.018	7.067	0.350	0.1324	0.0024	0.93	2110	83	2120	44	2130	32
Ku08-13-2	0.368	0.012	6.432	0.242	0.1266	0.0021	0.90	2022	59	2037	33	2051	29
~1 Ga													
Ku07-3-1	0.180	0.011	1.836	0.129	0.0741	0.0027	0.86	1065	59	1058	46	1044	74
Ku07-31-1	0.168	0.008	1.697	0.084	0.0733	0.0013	0.93	1001	43	1007	32	1022	36
Ku07-39-1	0.175	0.007	1.760	0.079	0.0731	0.0012	0.94	1037	40	1031	29	1017	33
~550 Ma													
Ku07-27-1	0.091	0.003	0.738	0.034	0.0587	0.0016	0.81	563	21	561	20	556	59
Ku07-41-2	0.089	0.005	0.719	0.045	0.0585	0.0022	0.81	550	27	550	27	549	82
Ku08-1-1	0.089	0.004	0.725	0.035	0.0587	0.0014	0.86	552	22	553	20	556	52
Ku08-3-1	0.088	0.004	0.710	0.036	0.0585	0.0015	0.86	544	23	545	21	549	56
Ku08-4-1	0.091	0.004	0.723	0.034	0.0579	0.0012	0.90	559	22	552	20	526	45
Ku08-10-1	0.090	0.004	0.729	0.034	0.0587	0.0015	0.84	556	21	556	20	556	56
~500 Ma													
Ku07-11-1	0.080	0.002	0.646	0.028	0.0588	0.0022	0.54	494	11	506	17	559	80
Ku07-23-2	0.083	0.003	0.656	0.038	0.0573	0.0027	0.60	515	17	512	23	503	104
Ku08-7-1	0.082	0.005	0.643	0.040	0.0572	0.0013	0.93	506	28	504	25	499	50

Table 3. Rb-Sr, Sm-Nd whole rock data and Pb-isotope ratios obtained on acid-leached K-feldspar from grey granites and red leucogranites I and II from the Kubas pluton.

	$^{87}Sr/^{86}Sr$ (m)	$^{87}Sr/^{86}Sr$ (i)	$^{87}Rb/^{86}Sr$	Rb (ppm)	Sr (ppm)	$^{143}Nd/^{144}Nd$ (m)	$^{147}Sm/^{144}Nd$	$^{143}Nd/^{144}Nd$ (i)
Red leucogranites I								
02/Ku01	1.947206(24)	0.7273	166.8	435.3	8.459	0.512426(10)	0.3791	0.511152
02/Ku02	1.711835(23)	0.7229	135.3	426.7	10.03	0.512268(07)	0.3358	0.511140
02/Ku03	1.958474(47)	0.7345	167.4	426.1	8.259	0.512547(03)	0.4270	0.511112
02/Ku04	1.556693(26)	0.7389	111.9	424.1	11.87	0.512046(06)	0.2727	0.511130
02/Ku05	3.622665(25)	0.7440	393.7	442.8	4.189	0.512648(09)	0.4503	0.511134
02/Ku06	1.464660(16)	0.7345	99.87	448.2	13.95	0.512388(13)	0.3796	0.511112
Red leucogranites II								
09/Ku01	0.823526(11)	0.7123	15.22	211.6	40.68	0.511880(01)	0.1781	0.511282
09/Ku09	0.811141(14)	0.7205	12.40	235.2	55.44	0.511943(03)	0.2225	0.511195
09/Ku11	1.101503(19)	0.7201	52.17	319.1	18.38	0.511894(01)	0.2667	0.510998
Grey granites								
02/Ku08	0.757758(11)	0.7197	4.851	248	145	0.511495(04)	0.1090	0.511100
02/Ku09	0.756033(10)	0.7187	4.760	235	140	0.511577(05)	0.1265	0.511119
02/Ku11	0.757818(09)	0.7184	5.033	236	133	0.511580(03)	0.1286	0.511114
02/Ku12	0.758407(10)	0.7198	4.923	243	140	0.511524(07)	0.1138	0.511112
09/Ku02	0.751152(19)	0.7187	4.135	248	170	0.511437(02)	0.1046	0.511058
09/Ku04	0.759106(12)	0.7199	5.005	247	140	0.511431(03)	0.1059	0.511047
09/Ku05	0.756103(16)	0.7203	4.561	230	143	0.511519(02)	0.1131	0.511109
*M64 **	*0.757412(09)*	*0.7175*	*5.097*	*239*	*133*	*0.511527(04)*	*0.11*	*0.511156*
*M68 **	*0.760666(10)*	*0.7151*	*5.812*	*254*	*124*	*0.511526(05)*	*0.11*	*0.511155*
*M73 **	*0.753718(10)*	*0.7163*	*4.773*	*234*	*139*	*0.511508(07)*	*0.11*	*0.511137*

Analytical methods are described in Appendix A. Uncertainties for the $^{87}Sr/^{86}Sr$ and $^{143}Nd/^{144}Nd$ isotope ratios are 2σ errors in the last two digits. Calculation of ε_{Nd} values is relative to CHUR according to Jacobsen and Wasserburg (1980). Nd model age (T_{DM}) calculation is according to Michard et al. (1985). Samples with $^{147}Sm/^{144}Nd > 0.13$ are corrected using the correction procedure of Milisenda et al. (1994).

* $^{87}Rb/^{86}Sr$ ratios are calculated from XRF-data; for $^{147}Sm/^{144}Nd$ a ratio of 0.11 is assumed. Both are not treated in the text.

Table 4. CIPW normative composition of the red leucogranites I and II and the grey granites. Values are calculated with the GCDkit program (Janoušek et al., 2006).

	Q	C	Or	Ab	An	Hy	Mt	Il	Hm	Ru	Ap	Sum
Red leucogranites I												
02/Ku01	33.41	1.00	27.24	33.59	2.42	0.10	0.43	0.02	0.47	0.00	0.10	98.77
02/Ku02	34.79	1.20	26.00	34.86	2.10	0.10	0.23	0.02	0.72	0.00	0.05	100.07
02/Ku03	34.74	1.02	25.77	34.78	2.55	0.10	0.43	0.02	0.58	0.00	0.05	100.01
02/Ku04	34.15	0.93	26.59	33.59	3.13	0.13	0.17	0.04	0.78	0.00	0.14	99.65
02/Ku05	34.24	0.84	24.82	35.54	3.06	0.10	0.33	0.02	0.53	0.00	0.02	99.51
02/Ku06	33.19	0.82	25.35	34.86	2.90	0.08	0.30	0.02	0.60	0.00	0.12	98.22
Red leucogranites II												
09/Ku01	32.88	3.17	27.60	31.82	1.88	0.50	0.51	0.10	0.61	0.00	0.45	99.51
09/Ku09	35.43	0.65	29.02	28.60	5.54	0.13	0.00	0.02	0.48	0.03	0.02	99.92
09/Ku11	35.39	0.62	25.59	33.42	4.09	0.13	0.00	0.04	0.52	0.04	0.05	99.88
Grey granites												
02/Ku08	30.80	0.91	25.53	27.33	9.25	2.14	0.00	0.11	2.55	0.31	0.19	99.13
02/Ku09	27.88	0.70	27.78	27.33	8.92	1.74	0.00	0.11	2.46	0.30	0.24	97.46
02/Ku11	30.13	0.95	28.13	26.57	8.43	1.77	0.00	0.11	2.48	0.29	0.24	99.10
02/Ku12	31.66	1.23	26.89	26.91	8.66	1.94	0.00	0.13	2.76	0.31	0.33	100.82
09/ku02	29.39	0.98	28.60	24.96	9.44	2.17	0.00	0.13	3.07	0.35	0.28	99.38
09/Ku04	31.82	2.11	26.12	26.74	7.57	1.99	0.00	0.13	3.02	0.33	0.26	100.10
09/Ku05	28.12	0.61	27.42	28.43	9.37	2.57	0.00	0.11	2.68	0.31	0.24	99.85
02/Ku07	28.83	0.73	24.53	28.35	9.39	2.07	0.00	0.17	2.69	0.30	0.28	97.33
02/Ku10	30.13	0.87	27.13	27.50	8.38	1.77	0.00	0.11	2.47	0.28	0.24	98.87
09/Ku07	30.39	1.45	27.36	26.23	8.21	2.52	0.00	0.11	2.69	0.32	0.33	99.61
09/Ku08	29.56	1.18	25.12	28.77	9.38	2.69	0.00	0.11	2.85	0.31	0.21	100.19
09/Ku10	29.65	0.71	27.60	27.59	8.44	2.32	0.00	0.11	2.55	0.28	0.28	99.53
M64	29.19	0.57	27.07	27.42	9.53	1.92	0.00	0.11	2.62	0.31	0.21	98.95
M66	28.86	0.72	27.07	27.42	9.68	2.09	0.00	0.11	2.60	0.31	0.21	99.08
M68	30.92	0.74	27.95	26.91	8.84	1.72	0.00	0.11	2.52	0.29	0.21	100.22
M70	31.46	0.58	29.84	25.39	8.66	1.74	0.00	0.11	2.56	0.29	0.19	100.82
M71	28.90	0.64	27.19	27.50	9.88	2.17	0.00	0.11	2.68	0.32	0.21	99.60
M73	27.17	0.54	28.01	27.08	9.62	2.24	0.00	0.13	2.81	0.32	0.24	98.16

Table 5. Temperature estimates for the grey granites based on Al/Ti systematics and apatite and zircon saturation thermometry.

	T_{Zr}	T_{Ap}	$T_{Al\text{-}Ti}$
02/Ku08	745	896	891
02/Ku09	781	900	888
02/Ku11	778	918	885
02/Ku12	787	964	892
09/Ku02	780	928	902
09/Ku04	806	930	895
09/Ku05	773	914	889
02/Ku07	801	918	897
02/Ku10	780	917	883
09/Ku07	786	951	892
09/Ku08	776	907	888
09/Ku10	765	938	883
M64	778	902	891
M66	774	901	890
M68	780	917	886
M70	781	912	887
M71	771	904	892
M73	772	899	895

(See text for details)

Highlights

Pan-African granite intrusion in the high-grade central part of the Damara orogen (Namibia)

High-temperature partial melting of meta-igneous basement rocks of Archean to Proterozoic age

Granite intrusion simultaneously with crustal thickening at c. 550 Ma, before the first peak of high-grade regional metamorphism

Formation of leucogranites during the main peak of regional metamorphism at c. 510 Ma